university of groningen / faculty of science and engineering / biomedical engineering

Finite Element Model Design for Articular Cartilage Creep Behavior

Wietse Kalisvaart
S4575687

15/07/2023

Faculty of Science & Engineering

Period: 06/02/2023 - 10/07/2023

Master Thesis

Daily Supervisor: dr. ir. R. Fluit

1st examiner: dr. ir. R. Fluit, Faculty of Science & Engineering

2nd examiner: dr. P.K. Sharma, Faculty of Medical Sciences

Contents

Abstract

Osteoarthritis (OA) has a high prevalence among the elderly and is characterized by the degradation of the articular cartilage (AC) in the joints. This degradation is known to lead to a loss in mechanical functioning of the joints, most commonly the knee joint, and is the leading cause for knee replacement surgery. With an increase in knowledge regarding the biomechanical behavior of degraded cartilage a model might be obtained to simulate the AC behavior based on the penetration depth of the degradation.

Creep and relaxation tests have been performed on healthy and enzymatically degraded cartilage. Collagenase III was added to the cartilage to degrade the collagen II fibers which maintain the structure of the AC and provide stiffness. Chondroitinase ABC was used to degrade the glycosaminoglycans (GAGs) which hold the water in the AC. Varying degradation times were used, namely 1 hour, 2 hours, 4 hours and 16 hours. The data was analyzed using Python and a viscoelastic model was fitted to the relaxation data of a healthy AC plug. A curve fit to the relaxation curves in Python was used to obtain the initial values which were used for the optimization of the Finite Element (FE) model.

Histology has been performed on the 4 hour and 16 hour degraded groups with a control. A penetration depth of 130 and 401 microns was discovered for the 4 hour and 16 hour groups of Chondroitinase ABC. No clear penetration depth was found for the collagenase III degraded groups.

A second layer was introduced to the FE model with a thickness matching the measured degradation depths. The 2-layered FE model was fitted to the relaxation curves of 4 hour and 16 hour GAG degraded AC and showed an increase in Young's Modulus for the 4 hour group and a decrease for the 16 hour group.

For the collagen degraded AC significance was found between the control group and the 16 hour degraded group with a p-value of $p=0.04762$ the end stress variable,which is the stress at the last second of relaxation. For the GAG degraded AC significance was again found between the control group and the 16 hour degraded group. A p-value of $p=0.00909$ was found for the peak stress of GAG degraded AC and a significance of $p=0.01818$ was found for the end stress. All the significant changes were rejected after a post-hoc test was performed.

Due to the limited number of datapoints for the degradation depth it was not feasible to find a trendline showing the penetration depth over degradation time. In future research it is recommended to use degradation times greater than 4 hours to ensure the material is being degraded. An increase in sample size is recommended as well, as the sample size for each group during the research was only $n=3$.

1 Introduction

Osteoarthritis (OA) has a high prevalence among the elderly and is characterized by the degradation of the articular cartilage (AC) in the joints [1]. This degradation is known to lead to a loss in mechanical functioning of the joints, most commonly the knee joint, and is the leading cause for knee replacement surgery.

Knowledge about the degradation behavior of the AC with OA is however still limited, which makes targeted treatment more difficult. Experiments regarding the degradation of AC under influence of OA have been researched by several groups with several different methods. For example, Halonen et al made use of a Finite Element (FE) model to predict the deformation of the knee joint under constant load[2]. Another method by Korhonen et al tried to mimic the degradation of cartilage using enzyme solutions with digestion time of 44 hours. Afterwards the effects on the biomechanical properties were observed[3]. Due to the limited times of degradation, namely 0 hours and 44 hours, no observations could be made regarding the penetration depth over time.

Although this research is already being done, many unknowns regarding the AC behavior still remain, such as the effect the penetration depth of the OA in combination with the type of breakdown on the biomechanical changes. With the addition of knowledge regarding this degradation behavior, new treatment options may be developed which could offer more targeted treatment of the OA or even cure the disease.

The aim for this thesis will be the characterization of the enzymatic breakdown of the AC and how this will affect the biomechanical behavior. A model will be created using the FE Method to predict the behavior of enzymatically degraded AC samples. Experimental tests will be done to first find the relationship between enzyme degradation time and penetration depth, and next to find the relationship between the penetration depth of the enzymatic breakdown and the biomechanical properties. Following the model, the biomechanical properties of AC, degraded to a specific depth, can be simulated and approximated. Due to the breakdown of the cartilage a reduction in strength of the material is expected.

Breakdown of the AC shall be conducted using two enzymes, which will degrade the proteoglycans and collagens in the material. A range of shorter degradation times shall be used as most research is focused on longer degradation times of 24 hours or longer. Focusing on the shorter times should give a clearer view of the degradation depth over time.

First a bit of background shall be given regarding the structure and biomechanical behavior of AC. Next several available FE models will be discussed in depth. Following this, the methods and materials used shall be explained and the flow of the experiment will be given. In the final chapters the results will be shown and discussed and a final recommendation will be given. The ethics regarding the acquisition of animal testing material will also be discussed.

2 Articular Cartilage

AC is a soft-tissue covering the places where bones interact with each other, providing the space with a low-friction and load-bearing area [4]. This area aids in the movement of the joint, as it allows the bones to glide smoothly over each other. This impressive behavior of the AC is mainly caused by its ability to retain water in its porous structure. Due to the proteins available in the AC, it is able to hold up to 70% of water, which aids the material in supporting compressive loads [4].

In order to create a realistic model of the AC, its structure and biomechanics should be properly researched. This chapter will be used to describe the different views in the structure of the AC and the different ways OA affects the healthy AC.

2.1 Structure

AC is typically 2 to 4 mm in thickness and can be separated in four different zones, the superficial zone, the middle zone, the deep zone and the calcified zone [4, 5, 6]. These zones consist of a combination of collagen, mainly collagen type II, proteoglycans and articular chondrocytes. The different concentrations of these proteins throughout the zones cause different mechanical and biological behaviors throughout the AC.

Collagen fibers provide the AC with compressive strength due to their arcade-like arrangement. In the deep zone these fibers are oriented perpendicular to the AC surface, in the middle zone they change their orientation to become more oblique, whilst in the superficial zone the orientation is parallel to the AC surface. This proposed structure gives an increase in compressive resistance throughout the layers, with the deep zone having the highest resistance to compression [6]. Furthermore, the thickness of the fibers have been found to increase with the depth of the AC, where the fibers in the superficial zone are thinnest [4]. A schematic overview of the proposed collagen fiber structure is displayed in figure 1.

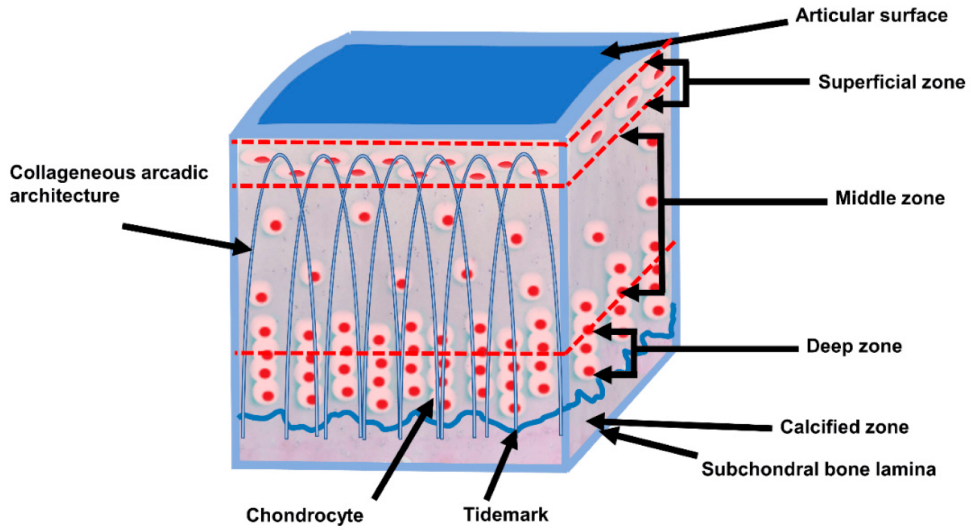

Figure 1: Cross-sectional diagram of articular cartilage (from Eschweiler et al[6])

Another model for the collagen fiber structures in the AC has been proposed by He et al. This model states that the superficial layers consist of several layers of collagen fibers parallel to the surface. The

cascading arches are thought to be in the deep and middle zone, with the tips of the arches touching the transitioning zone between the middle and superficial zone [5]. An image showing this model can be seen in figure 2. Moreover, figure 3 shows images obtained using second harmonic generation, which show the distribution of collagen fibers throughout the AC in the transverse and longitudinal view.

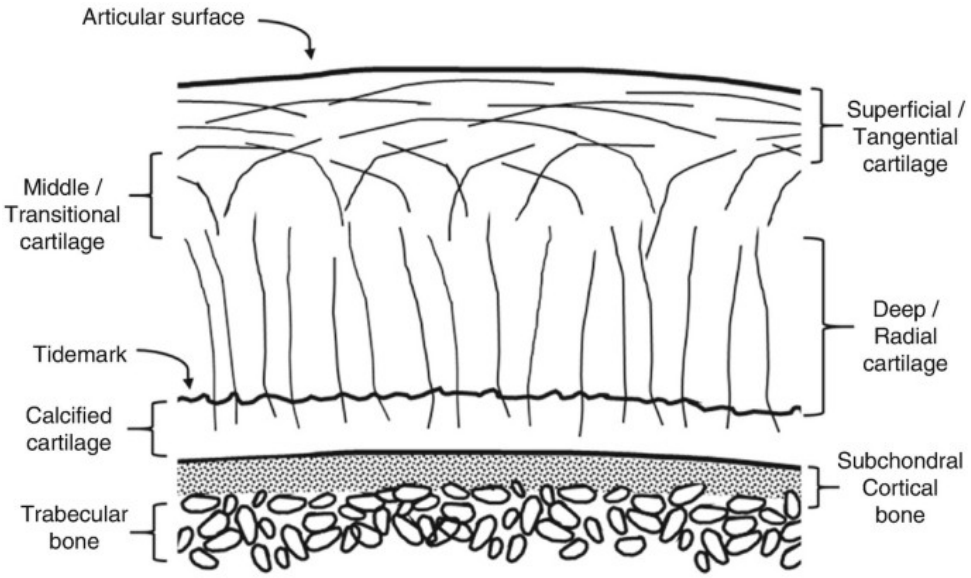

Figure 2: Cartilage structure as proposed by He et al[5] (from Chappel et al[7])

Image D in figure 3 shows the proposed structure by He et al. It clearly shows a horizontal orientation of the collagen fibers in the upper layer. The middle zone shown in image D shows the cascades of collagen fibers and the fibers in the deep zone are oriented perpendicular to the surface of the cartilage, as seen in figure F.

The proteoglycans in the AC consist of long chains of sugar called glycosaminoglycans (GAGs). Thanks to the positive charge of these proteoglycans, water can bound easily to the structures [6, 8, 9]. On compression, some of the water will be released, providing lubrication of the joint. On relaxation, the expelled water will diffuse back into the AC and the equilibrium will be restored.

Chondrocytes are the highly specialized cells inside the AC, which play a role in the development, maintenance and repair of the extracellular matrix (ECM) [4, 6]. Throughout the zones, the chondrocytes are interwoven in the ECM and collagen fibers, causing the changes in shape. Due to the finely packed collagen fibers in the superficial zone, the chondrocytes have a flat, elongated shape. In the middle and deep zone, these cells become more rounded and lower in density, with the chondrocytes in the deep zone being vertically packed between the thick, perpendicular collagen fibers. Due to the way the micro environment traps the chondrocytes, they are rarely known to form cell-to-cell contact for direct communication and rely more on indirect stimuli, such as growth factors, loads and pressures. [4].

Other compounds in the structure of AC include mineral-like materials and matrix proteins. Table 1 has been supplied showing the approximate concentrations of each of the compounds in AC.

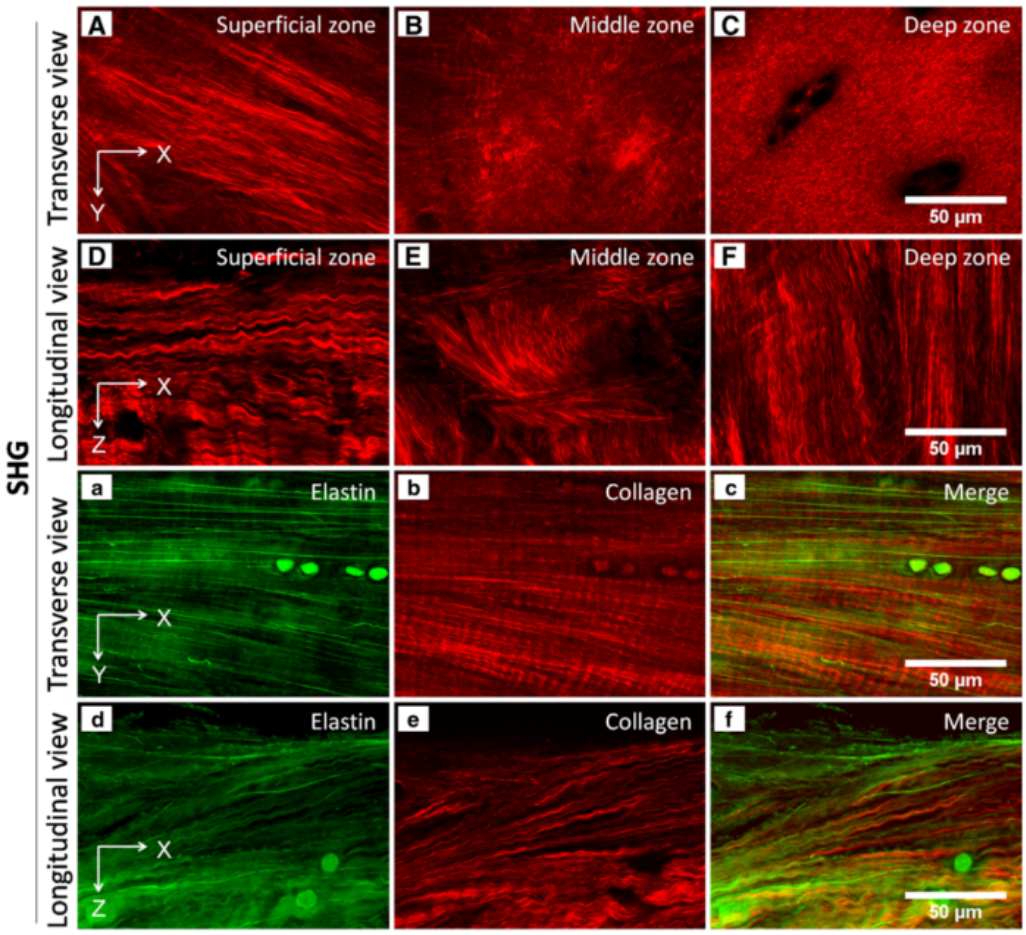

Figure 3: Second harmonic image of AC (from He et al[5])

Table 1: AC contents, adapted from He et al.[5]

Chondrocytes	1-10%
Water	70-80%
Collagen type II	10-12%
Collagen type IX	±1%
Collagen type XI	±1%
Proteoglycans	7-9%
Mineral-like Materials	±1%
Matrix proteins	<1%

2.2 Biomechanics

AC is generally considered to have two phases, a liquid phase and a solid phase. Due to the high water retention in the AC, any loads placed on the material are resisted by the liquid displacement in the material. As the fluid is compressed, it will move throughout the ECM of the AC with a certain porosity. During compression however, the porosity of the ECM is known to decrease due to the compression of the pores [10]. This mechanism is also called the flow-dependent mechanism of viscoelasticity. The flow-independent mechanism for viscoelasticity comprises of the changes in the

ECM structure, mainly the effect of the collagen and proteoglycan structures [6, 10].

This viscoelasticity caused by the flow-dependent and flow-independent mechanism causes the typical creep behavior that is seen during AC compression. The first onset of the load will cause a big water displacement, which results in quick deformation of the material. As the material becomes more compressed, the water content in the AC becomes reduced. This and the reduction in porosity of the matrix caused by the sudden deformation cause an increased resistance to the load. With the application of a constant load or stress, the AC will reach an equilibrium after a certain amount of time. The deformation behavior of AC under constant load or stress is called the creep response. The leftmost plots in figure 4 show a typical creep response for AC.

When a constant strain is applied to the AC, the viscous behavior of the material will resist the sudden change at first, but over time this resistance will decrease as the fluids in the AC are free to move and distribute over the material. The stresses placed on the material follow the typical stress-relaxation response as given by rightmost plots in figure 4.

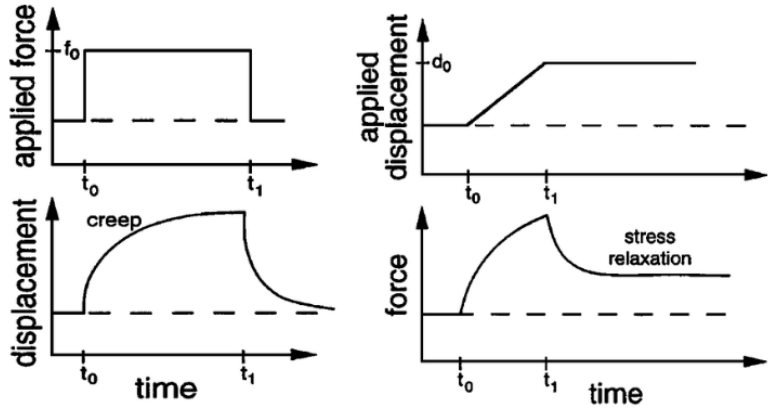

Figure 4: Creep and relax behavior of articular cartilage under constant strain and constant load (from Mow et al[11])

The typical behavior of AC as discussed in the previous chapters is however prone to degradation in the case of osteoarthritis. This disease is known to cause small lesions on the surface of the AC, which increase the friction of the joint and increase discomfort for the patient. Moreover, these lesions can cause further breakdown of the AC, requiring full-knee replacement for the patient.

Alternative treatments for osteoarthritis are highly sought after and there are some studies that focus on restoring the AC using stem cells [12]. Due to the highly specialized nature of the chondrocytes, restoring AC does however prove difficult and any damage caused by osteoarthritis remains permanent [1, 12].

3 Finite Element Modeling

FE Modeling is a useful tool for modeling complex material behavior. It works on the principle of subdividing a complex shape needing many differential functions to model, to a collection of smaller simpler shapes called finite elements. Each finite element is then used to approximate the field variables in the existing system[13]. This could for example be the deformation of a steel beam when a force is applied at one end.

The simulation software which is used, COMSOL, provides several different options for models. Several available simulations are heat transfer, fluid flow and solid mechanics. Moreover, COMSOL provides the possibility to combine multiple simulation types into Multiphysics problems. This will link the field variables between two or more different simulation types, ensuring they are influenced by one another. Although this will result in a more realistic approximation of the physics in the system, the computation time will greatly increase as more calculations are required to come to a solution.

For the purpose of modeling AC behavior under stress, several simulation types can be useful. Firstly, to model the compressive behavior of the AC the solid mechanics simulation can be used. This simulation can model the changes in shape of a material under applied stresses and also allows modeling of contact behavior between two objects. Using this feature, an indentation of the AC can be modeled under a constant load or strain. In addition fluid mechanics can be used in combination with solid mechanics to simulate the displacement of the water inside the AC during indentation.

There exist several different methods of modeling AC behavior. One method models all the behavior in a single continuum, which reduces the computation time, but simplifies the solid-fluid interactions significantly. These models are called monophasic and make use of the viscoelastic behavior of the material. When the fluid interactions are also included in the model, it is called a biphasic model. This type of model will make use of the poroviscoelastic behavior of the material, where in addition to the viscoelasticity of the material, the fluid flow throughout the pores inside the material is also considered[14, 15]. Other models can also include the fiber structures within the material, or might model the osmotic swelling that occurs inside the AC[3, 14]. For this thesis both the viscoelastic model and the poroviscoelastic model have been selected and implemented. These specific models will be further specified in the following chapters.

3.1 Viscoelastic Model

For viscoelasticity two different models are used to simulate the behavior of the material. First of all the Maxwell model can be used. This model consists of a spring and dashpot configuration, where both are placed in series with one another. The spring is used to simulate the elastic behavior following Hooke's law, while the dashpot simulates the viscous behavior of the material using Newton's law of viscosity[16, 17]. Figure 5 shows a typical Maxwell model. η indicates the viscosity and E indicates the stiffness of the material.

Since the Maxwell model consists of the two elements in series, the response to a strain applied to the model is affected by a combination of the linear stress of the spring and the time dependent stress of the dashpot, causing the typical relaxation behavior of AC as shown in figure 4. This makes the Maxwell model best suited for modeling the stress-relaxation behavior of AC.
The formula for Hooke's law is given by equation 1 and the formula for Newton's law of viscosity

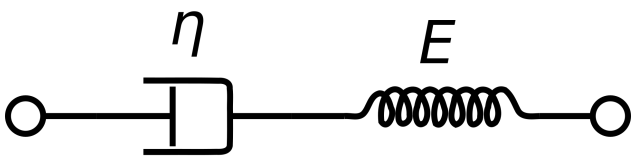

Figure 5: Maxwell model containing a spring and dashpot in series[18]

is given by equation 2[16]. Subscripts are added to the stresses and strain to indicate the linear part (subscript l) and the time-dependent part (subscript d).

$$\sigma_l = E \cdot \varepsilon_l \tag{1}$$

$$\sigma_d = \eta \cdot \dot{\varepsilon_d} \tag{2}$$

- σ = stress acting on the material
- ε = strain acting on the material

As the elements are placed in linear fashion, the total stress and strain become products of the stresses and strains given by equation 1 and 2 as shown in equation 3 and 4.

$$\varepsilon = \varepsilon_l + \varepsilon_d \tag{3}$$

$$\sigma = \sigma_l + \sigma_d \tag{4}$$

Following the instructions as given by Schippers et al[16], the equation for the Maxwell formula can be obtained by the transformation of equation 1-3. The formula is given in equation 5.

$$\dot{\varepsilon} = \frac{\dot{\sigma}}{E} + \frac{\sigma}{\eta} \tag{5}$$

Considering the relaxation test is performed at constant strain, the strain rate is zero. These conditions are shown by equation 6 and 7. Solving the Maxwell equation with these conditions, the relaxation equation given by equation 8 can be found. A variable τ is introduced to replace $\frac{\eta}{E}$.

$$0 = \frac{\dot{\sigma}}{E} + \frac{\sigma}{\eta} \tag{6}$$

$$\frac{d\sigma}{\sigma} = -\frac{E}{\eta} dt \tag{7}$$

$$\sigma(t) = \sigma_0 \cdot \exp(-\frac{t}{\tau}) \tag{8}$$

Another possible model that can be used is the Kelvin-Voigt model. Like the Maxwell model this model also consists of a combination of a spring and a dashpot. In this model they are however placed in parallel. Figure 6 shows a typical Kelvin-Voigt model.

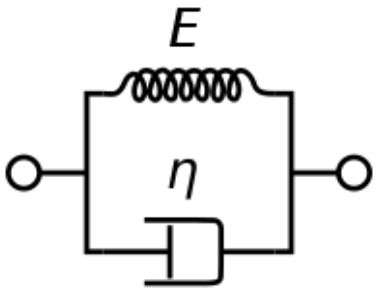

Figure 6: Kelvin-Voigt model containing a spring and dashpot in parallel[19]

Since the spring and dashpot are placed in parallel the strain is identical across both elements unlike the Maxwell model where the stress is identical. Thanks to this, the brunt of the force is received by the dashpot, causing the stress to gradually transfer to the spring. The differential equation showing creep behavior is given by equation 9. The solution for this equation is given by equation 10[17].

$$\frac{\sigma_0}{\eta} = \frac{\varepsilon}{\tau} + \dot{\varepsilon} \tag{9}$$

$$\varepsilon(t) = \frac{\sigma_0}{E} \cdot [1 - \exp(-\frac{t}{\tau})] \tag{10}$$

Due to the gradual transfer of the forces to the spring, the gradual increase in strain as is characteristic for creep is obtained, making the Kelvin-Voigt model suitable for simulating the creep of AC.

3.2 Poroviscoelastic Model

The addition of Darcy's law to the viscoelastic model will transform the viscoelastic model to a poroviscoelastic model. These models will also include the displacement of the fluids inside of the material, also simulating the viscous behavior of the fluid, which will influence the stress and strain on the AC.

Darcy's law is used to determine the pressure gradient, fluid viscosity and the structure of the porous medium[20]. The formula is shown in equation 11.

$$u = -\frac{k}{\mu} \nabla p \tag{11}$$

- u = Darcy's velocity
- k = permeability of porous medium
- μ = dynamic viscosity
- p = pore pressure

The gravity can also be taken into account by replacing ∇p with $(\nabla p + \rho g)$, where g is the gravity constant and ρ is the fluid density.

4 Methods

This chapter will focus on all the methods used during the thesis. First the preparations of the materials and solutions shall be discussed. Next the experiments and their testing setups shall be given. Following this the statistics used for the data is explained. Next a brief explanation is given regarding the histology done during the research and finally a section is dedicated to parameter fitting of the simulation data.

4.1 Preparation of materials

Several materials had to be prepared for the experiments. Firstly the cartilage plugs had to be obtained and secondly all solutions required for the experiments had to be prepared. Both shall be discussed in order to give a clear understanding of the methods used.

4.1.1 Preparation of cartilage plugs

In order to obtain sufficient cartilage plugs, two bovine knees were obtained from Kroon Vlees[21] for each experiment day. The bovine knees were brought to the UMCG, where the femoral condyles were extracted. These condyles were kept lubricated using a 7.0 pH PBS solution, which was prepared the previous day. Two condyles were obtained from each knee, coming to a total of 4 condyles. A picture of the obtained AC condyles is shown in figure 7.

Figure 7: AC condyles in PBS solution obtained from bovine knees

Following the extraction of the condyles, cartilage plugs were drilled from the condyles using a 12 mm diameter cylindrical drill. From each condyles three plugs were extracted, resulting in a total of

12 cartilage plugs. Figure 8 shows a reference picture of a cartilage plug. The plugs were stored in 7.0 pH PBS solution at a temperature of 8 degrees Celsius overnight before the enzymatic solutions were placed in the samples. A total of four bovine knees were required to obtain sufficient plugs for all groups, namely a 1 hour, 2 hour, 4 hour and 16 hour degradation group for both collagen and GAG degradation.

Figure 8: Reference image of an AC plug (from Hospital Innovations[22])

4.1.2 Preparation of solutions

Several solutions were prepared for the experiments. PBS was made to supply the cartilage with nutrients and lubrication for safe storage. Collagenase III and chondroitinase ABC were obtained to degrade the different proteins in the cartilage and ethylenediaminetetraacetic acid disodium salt dihydrate (EDTA) solution was obtained to decalcify the remaining bone in the cartilage sample to ease slicing of the material. Table 2 shows an overview of all the solutions with their concentrations and origin, if known.

PBS at pH 7.0
First of all, PBS was made following the standard procedures. The pH of the solution was corrected to a pH of 7.0 by the addition of KOH to the solution.

Collagenase at 50 ug/mL
Before adding the enzyme, antibiotics were added to 30 mL of PBS. Bovine Serum Albumin was selected and a total of 3.0 mg was added to the solution to create a PBS solution with 0.01% added BSA. To obtain the concentration of 50 ug/mL, 1500 ug of collagenase type III from Stemcell technologies was added to the solution and gently stirred by hand until all the enzyme was dissolved in the solution. The solution was stored at a temperature of -10 degrees Celsius until used.

Chondroitinase ABC at 0.1 U/mL
Following the same procedure used for collagenase, 30 mL of PBS containing 0.01% BSA was acquired. 3 units of chondroitinase ABC from Sigma Aldrich were added to the PBS solution and gently stirred until all the enzyme was dissolved. The solution was stored at a temperature of -10 degrees Celsius until used.

EDTA 10%
1 L of PBS buffer was prepared at pH 8.0 and 100 g of EDTA was added to the solution. The solution was then stirred until all the EDTA was dissolved into the liquid. The addition of EDTA to the PBS solution caused the pH to lower and after the solution was completely dissolved the pH was brought back to 8.0 with the addition of KOH. The obtained EDTA 10% solution was then stored at a temperature of 8 degrees Celsius.

Table 2: Overview of the procured solutions

Solution	**Concentration**	**Manufacturer**	**CAT**
PBS	n/a	n/a	n/a
Collagenase III	50 ug/mL	Stemcell Technologies	07422
Chondroitinase ABC	0.1 U/mL	Sigma Aldrich	C3667
EDTA	10%	n/a	n/a

4.2 Experiments

The experiments will be conducted using the Universal Mechanical Tester (UMT) by Bruker. The machine is shown in figure 9. This machine allows tribology testing of materials at a wide range of forces. By changing the load cells in the machine, the forces acting on the material can be measured at varying precision. For the stress relaxation and creep tests a 10N load cell was placed on the machine. This load cell allows measurements of up to 10N by the UMT. Safety is built-in to disengage the material when these forces are exceeded to prevent damaging the load cells.

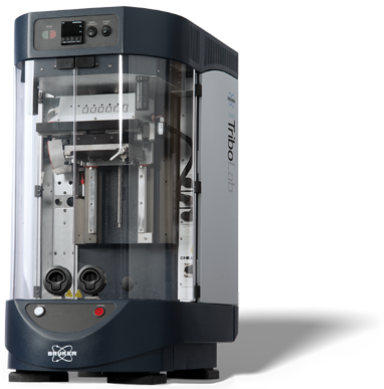

Figure 9: UMT tribolab by Bruker (from Bruker[23])

The UMT allows measurements of the forces in 3 axes and also has the ability to calculate the coefficient of friction of the material. The machine has three motors, which allow the machine to move up and down, left to right, and front to back. For the experiments the machine is centered above the material and only the vertical motor will be used.

4.2.1 Test setup

An aluminum ball with a diameter of 6.3 mm was mounted on top of a glass panel. The panel was placed on the bottom of a container, which was filled with pH 7.0 PBS solution heated to a temperature of 38 degrees Celsius. The cartilage plugs were mounted in a cylindrical holder attached to the UMT and lowered into the PBS bath before starting the UMT tests. A schematic view of the proposed test setup is shown in figure 10. Figure 11 shows an image of the test setup loaded with an AC condyle.

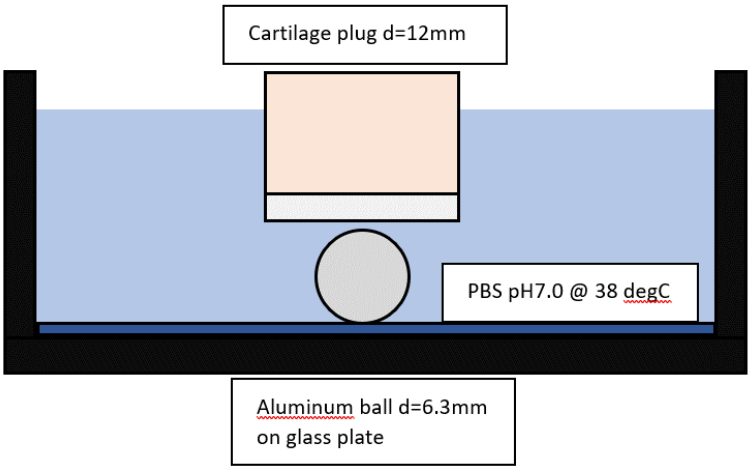

Figure 10: Testing setup for creep and relaxation experiments

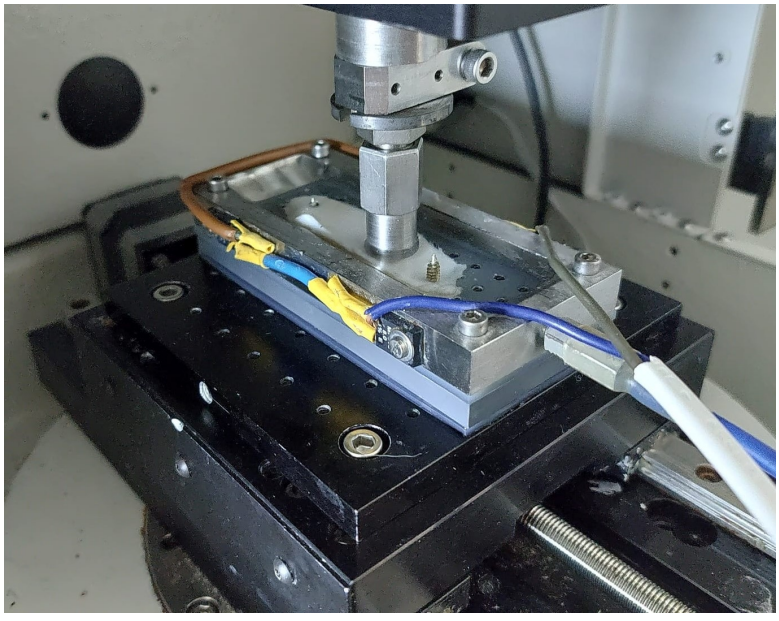

Figure 11: UMT setup showing the PBS bath with heater, indenter and mounted condyle

4.2.2 UMT configuration

Two different UMT routines were created for a relaxation test and creep test respectively.

The relaxation test applies controlled displacement to the cartilage plugs. Before the test, the thickness of the plug is measured and displacement is set to 10% of the measured thickness. As such, a strain of 10% will be applied to the AC. The plug is first lowered until a force of 0.1 N is detected to ensure a connection between the aluminum ball and the plug. Next the the plug is lowered into the aluminum ball to a depth corresponding to 10% strain during a time duration of 2.5 seconds. Finally the position of the plug is held constant during the next 60 seconds and the contact forces over time are measured. A graphical representation of the protocol is given by figure 12.

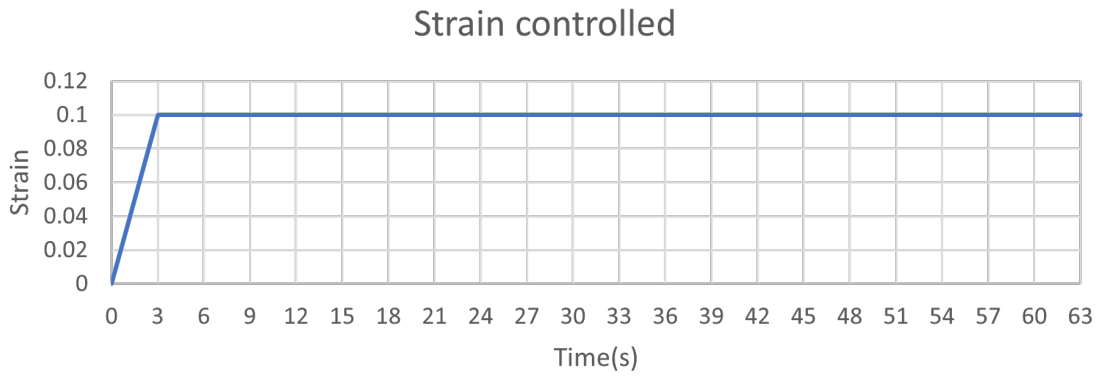

Figure 12: Controlled indentation of the AC

Contrary to the relaxation test, the creep test applies controlled forces to the cartilage plugs. Again contact is ensured by lowering until a force of 0.1 N is detected, after which the force is increased to 4 N over a time of 45 seconds. This force is kept constant during a time duration of 7.5 minutes. Next, the controlled force is lowered to 0.1 N during a time duration of 3 seconds. This force is also kept constant during a time duration of 7.5 minutes. During the test, the vertical position of the cartilage plug is monitored to track the creep behavior of the material. A graphical representation of the protocol is given by figure 13

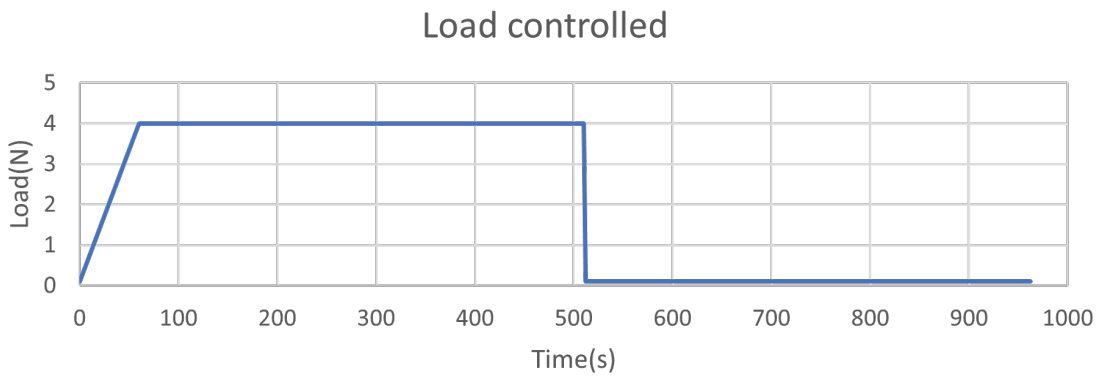

Figure 13: Controlled loading of the AC

4.2.3 Data analysis

The UMT data was exported to csv files and imported into Python. Functions were made to convert the data format of the UMT files to a suitable format and saved to a Pandas DataFrame. Two UMT files were created for each plug, namely the data for the creep and relaxation test. Using the loading step for the relaxation data, the stress-strain curve is also created and saved to the DataFrame. As such, each plug is saved in the DataFrame with its corresponding label, creep data, relaxation data and stress-strain curve. Before the data is converted, the starting strain, which is induced by the UMT when ensuring contact, is approximated by fitting a linear function to the stress-strain curve. Equation 13 shows the linear function that was used. The linear function is assumed to pass through the point (0,0), as zero stress is expected at zero strain. An optimization algorithm is used to minimize the 'strain' variable in the equation to find the starting strain with which the fitted linear function passes through the (0,0) point. The value of the 'stiffness' variable is saved and gives an approximation of the stiffness of the material. The found starting strain is used to correct the creep and relaxation data, as the change in strain will affect the contact area between the indenter and the cartilage, and as such also affect the calculated stresses on the material.

Hertzian contact theory is used approximate the contact area between the indenter and the AC. The formula for the contact area between a rigid indenter and a half-plane is given by equation 12[24]. A picture illustrating the indentation and showing the Hertzian contact area 'a' is given in figure 14.

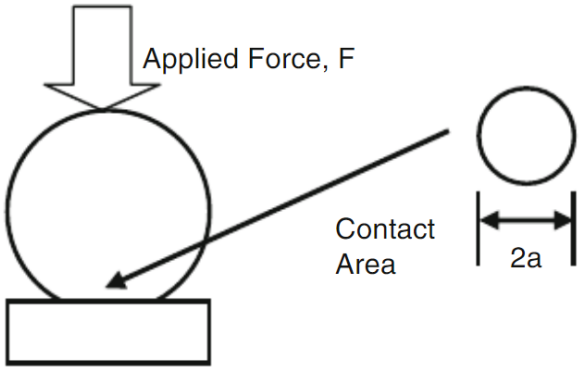

Figure 14: Indentation of half-plane with rigid indenter (from Ghaednia et al[25])

$$a = \sqrt{Rd} \tag{12}$$

- R = radius of indenter
- d = penetration depth

The effects of the preliminary approximation of the starting strain are shown in figure 15. As can be seen from figure 15a, without correction the stress starts at a very high value and reduces as the strain is increased. This should however be the opposite, as the stress should increase as a larger strain is introduced. Figure 15b has the strain correction applied to the data and does show this behavior. Furthermore, the fitted line shows the linear part of the stress strain curve passes through the (0,0) point.

$$f(x, stiffness, strain) = stiffness \cdot x + strain \tag{13}$$

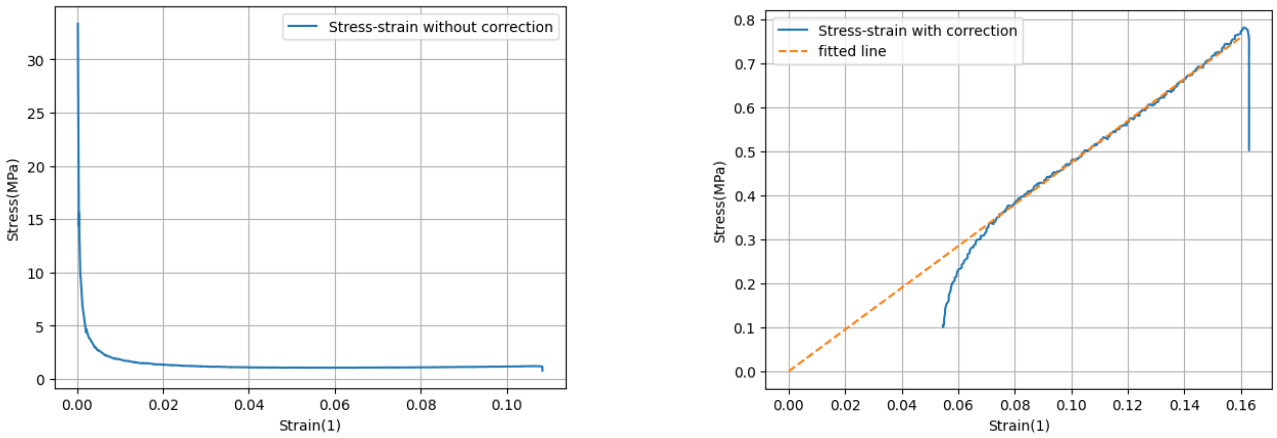

(a) Raw data

(b) Data corrected for starting strain

Figure 15: Stress strain curves for a 16 hour GAG degraded AC plug

From the data that has been corrected for the starting strain several variables are obtained. An overview of the variables is given in table 3.

Table 3: Overview of the obtained variables

Variable	**Unit**	**Origin**	**Description**
Stiffness	MPa	Relaxation test	Stiffness of the material obtained from the stress-relaxation plot
Peak Stress	MPa	Relaxation test	Maximum stress measured by the UMT
End Stress	MPa	Relaxation test	Stress measured by the UMT at the final second of the test
τ Stress	s	Relaxation test	τ found in the curve fitting step of the data
Stress Reduction	%	Relaxation test	percentile reduction of the stress from peak to end
Peak strain	-	Creep test	Maximum strain measured by the UMT
End Strain	-	Creep test	Strain measured by the UMT at the final second of the test
τ Strain	s	Creep test	τ found in the curve fitting step of the data
Strain Reduction	%	Creep test	percentile reduction of the strain from peak to end

4.3 Statistics

Due to the limited dataset of 3 samples per group, a Man Whitney U test was selected for testing the significance of the data. The cutoff has been chosen as p=0.05 to indicate significance. Since the groups are of limited size, a normal distribution cannot be assumed for them and as such, an ANOVA test will be based on wrong presumptions. The test accounts for the lack of a normal distribution and will give more reliable results. An F-value and p-value can be obtained from the test. The F-value is often used for analyzing the variance of groups.

In order to find the critical F-value, the numerator and denominator degrees of freedom (DOF) are needed. Equation 14[26] shows the formula for calculating the numerator DOF and equation 15[27] shows the formula for the denominator DOF. Filling these formulas for the dataset, a numerator DOF of 4 and a denominator DOF of 21 were found. The critical value can now be found from the F-distribution tables[28]. From the table a critical F-value of $F_{(4,18)} = 2.9277$ was obtained. When the obtained F-value is higher than this critical F-value, the null hypothesis can be rejected. The calculated p-value is influenced by the found F-value and is leading in rejecting the null hypothesis.

$$D_{fn} = N - 1 \tag{14}$$

- D_{fn} = degrees of freedom numerator
- N = number of samples

$$D_{fd} = N - k \tag{15}$$

- D_{fd} = degrees of freedom denominator
- k = number of groups

Considering several tests are to be run for many different features obtained from the dataset, a post-hoc test needs to be done to ensure that found significance does not occur by chance. For the post-hoc test the Holm-Benferroni equation was used[29]. Equation 16 shows the algorithm used. First the results from the Man Whitney U test are ordered from most significant to least significant. The rank of 1 is given to the most significant p-value and increases by one for each subsequent p-value. Using the rank the corrected target p-value can be calculated. The calculated p-value is then compared to the corrected target p-value and if it is still below the cutoff, the null hypothesis remains rejected.

$$HB = \frac{\alpha_t}{n - rank + 1} \tag{16}$$

4.4 Histology

To find the penetration depth of the enzymes the samples will have to be preserved. Several steps have to be taken to prepare the material for histology.

4.4.1 Preparing the samples for staining

After experiments had been conducted on the materials, they were placed in formaldehyde 4% for a duration of 3-5 days, after which the materials were rinsed using PBS and had the excess of bone removed. Since the bony parts in the cartilage samples could not be cut, the materials were also decalcified using a 10% EDTA solution. The samples were stored at a temperature of 8 degrees Celsius for a period of 2-4 weeks during which the solution was replaced weekly. After the materials were decalcified they were encased in wax and slices were cut at a thickness of 5 um. A selection was made consisting of the 4-hour and 16-hour degradation groups with a control group. Each group consisted of two slides, to allow staining for both collagen structures and GAGs using Alcian blue and H&E respectively.

4.4.2 Staining

The obtained slides were labeled and given to the histology department to be stained using Alcian blue and H&E staining. After staining, images were taken with a microscope at a resolution of 411 pixels per 200 um. The obtained images were imported into GIMP, an open source photoshop application, to calculate the total penetration depth using the given resolution.

4.5 Parameter fitting for models

From the experimental data two optimizations were performed. One optimization was done in Python and the other was done using COMSOL. Both optimization methods shall be thoroughly discussed.

4.5.1 Fitting parameters in Python

Following the Maxwell equations, the relaxation curve was fitted to the relaxation data in Python. The relaxation curve was plotted to the relaxing step in the relaxation test, namely where the indentation was kept constant over a period of 60 seconds. Equation 17 shows the formula to which the relaxation curve has been fitted[30]. G is the shear modulus of the material, G_m is the shear modulus of each additional branch of the Maxwell model and τ_m is the relaxation time related to the additional branches. Figure 16 shows a graphical representation of the Maxwell model that was implemented. The formula was fitted for $m = 2$ branches with an offset of 2.5 seconds in the time to account for the loading step of the relaxation test.

$$\Gamma(t) = G + \sum_{m=1}^{N} G_m \cdot \exp\left(\frac{-t}{\tau_m}\right) \tag{17}$$

The shear stresses and relaxation times found from the curve fits have been used as initial guesses for the optimization of the COMSOL model, which is also capable of modeling the loading step of the relaxation test.

4.5.2 Fitting parameters in COMSOL

A connection was set up between COMSOL and Matlab. The relaxation curve for the desired cartilage plug was loaded into Matlab. A linear viscoelastic model was selected and the fmincon function of Matlab was used for the optimization[31]. The optimization algorithm tries to minimize the output of a function f(x) using the algorithm shown in figure 17[31]. The function passed to the fmincon optimization algorithm sets up the Maxwell variables in the COMSOL simulation and changes the

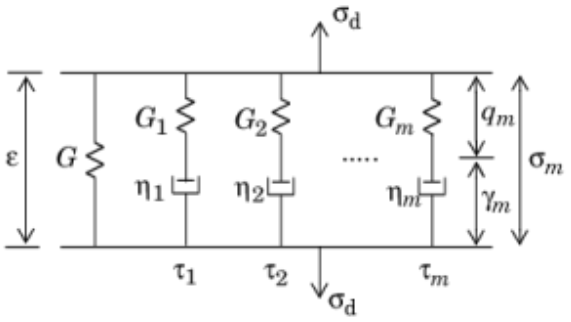

Figure 16: Generalized Maxwell model[30]

simulation runtime to t=45 seconds for time saving purposes. After the simulation is finished, the stress at 0.1 second intervals is read and compared with the imported experimental data. The function will then return the Root Mean Square Deviation(RMSD) to the fmincon algorithm. The equation used to obtain the RMSD is given by equation 18. x_e corresponds to the datapoints from the experimental data and x corresponds to the datapoints obtained from the COMSOL simulation. The fmincon algorithm will try different Maxwell variables until a local minimum is detected. The found parameters are then imported into the COMSOL simulation and run for the full time duration.

$$\min_x f(x) \text{ such that } \begin{cases} c(x) \leq 0 \\ ceq(x) = 0 \\ A \cdot x \leq b \\ Aeq \cdot x = beq \\ lb \leq x \leq ub, \end{cases}$$

Figure 17: Fmincon algorithm (from Matlab[31])

- x = function variables vector
- c(x) = array of nonlinear inequality constraints
- A = linear inequality constraints matrix
- b = linear inequality constraints vector
- Aeq = linear equality constraints matrix
- beq = linear equality constraints vector
- lb = lower bounds vector
- ub = upper bounds vector

$$f(x) = RMSD = \sqrt{\frac{\sum_{m=1}^{N}(x_e - x)^2}{N}} \tag{18}$$

5 Results

After the experiments have been conducted following the methods explained in chapter 4, several different results have been obtained. This chapter will be used to show the results and give some information regarding them. First the data obtained from the data analysis shall be discussed. Next the histological images will be shown and finally the results of the COMSOL models shall be given.

5.1 Data analysis

The data received from the UMT was imported into the Python software and converted to usable formats. The separate time steps are combined into one dataset and the stresses were calculated from the given indentations and loads. The groups were separated into a collagenase and chondroitinase ABC group, each consisting of two control, a 1 hour degradation, a 2 hour degradation, a 4 hour degradation and a 16 hour degradation group. For each group the average values were plotted with error bars displaying the standard deviation of the groups.

The average creep of the collagen and chondroitinase ABC degraded AC are given by figure 18 and 19. Both the collagen and chondroitinase ABC group show an increase in strain when the degradation time is increased. Furthermore, it can be observed that there is a lot of deviation within the groups, although this deviation appears to decrease as the degradation time is increased. One last observation that can be made is that during the loading phase there appears to be a slight increase in the strain around $t = 50s$ for some of the curves.

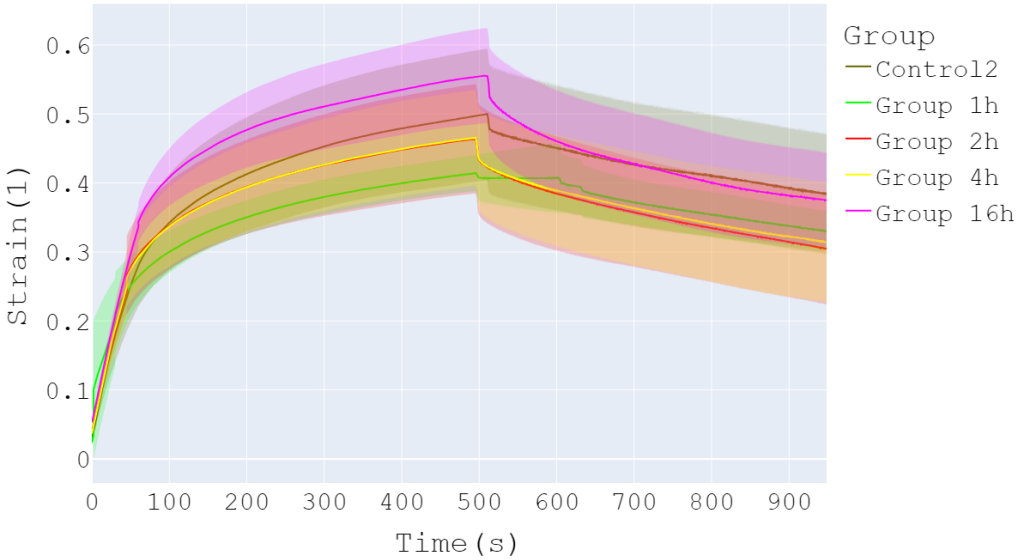

Figure 18: Average creep of collagen degraded AC over time per group

The obtained relaxation curves for the groups are given in figure 20 and 21. These figures show the stresses measured by the UMT over time. The relaxation curve for the groups are clearly shown by the graph. A reduction of stresses for the 16 hour degraded groups can be observed. The other groups did not appear to have had much deviation from the control groups, as all except for the 16 hour

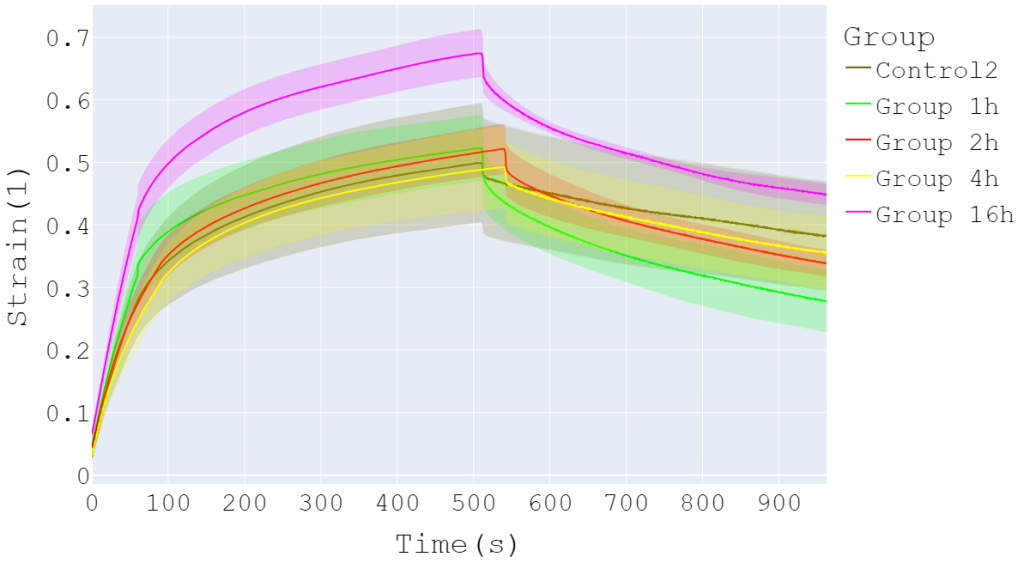

Figure 19: Average creep of GAG degraded AC over time per group

groups appear to be within one standard deviation of them. All groups seem to end at similar stresses, although the 16 hour degraded groups appear to decrease to a slightly lower end stress.

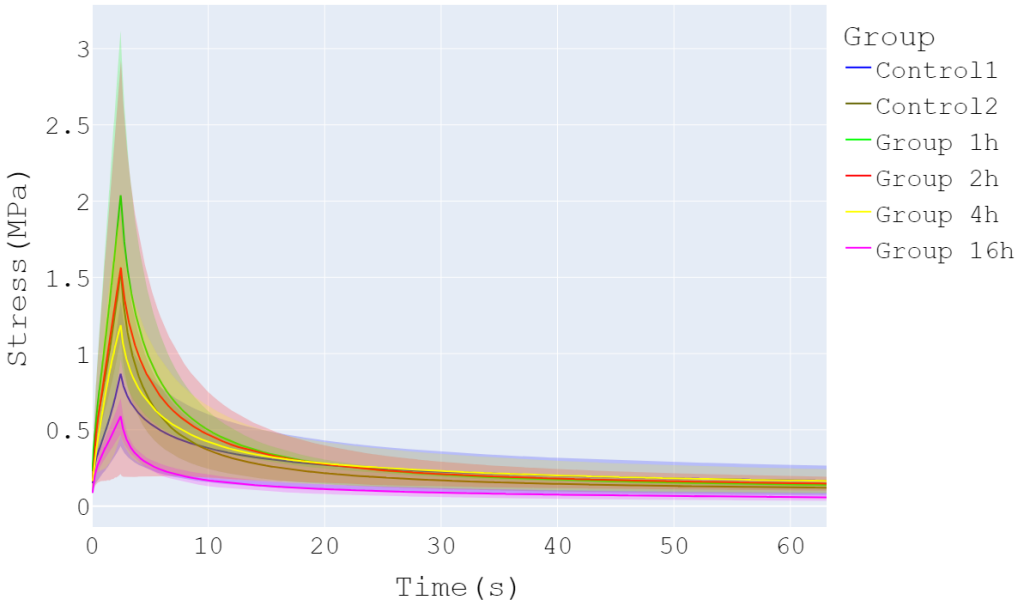

Figure 20: Average relaxation of collagen degraded AC over time per group

From the curves given by figure 18-21 the variables as given by table 3 were obtained for each of the plugs. From these values the averages and their respective standard deviations were calculated. The biggest changes were observed in the average stiffness, peak strain, peak stress and end stress. These

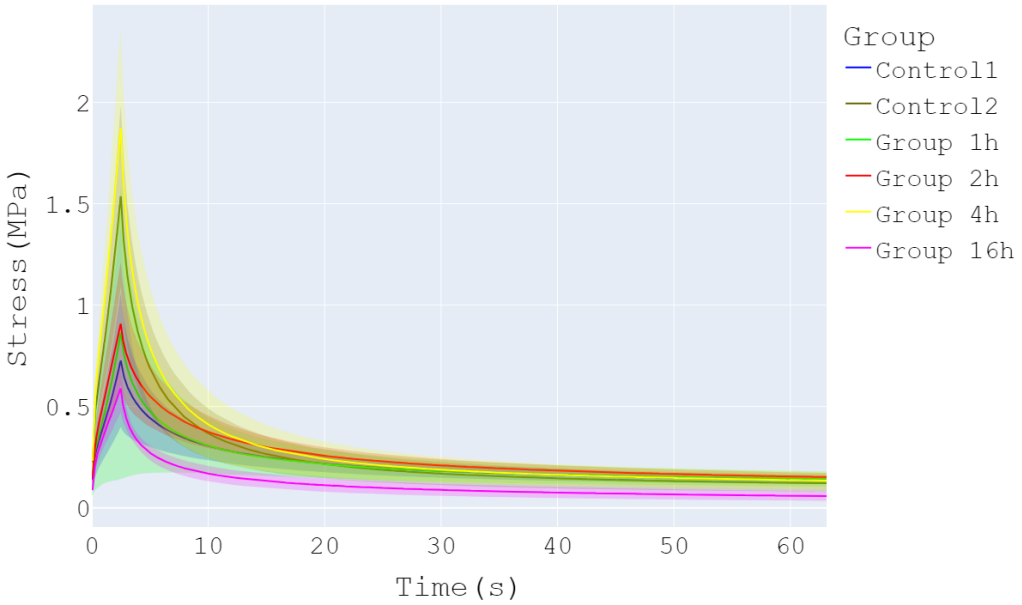

Figure 21: Average relaxation of GAG degraded AC over time per group

values are given by figure 22 for the collagen degraded AC.

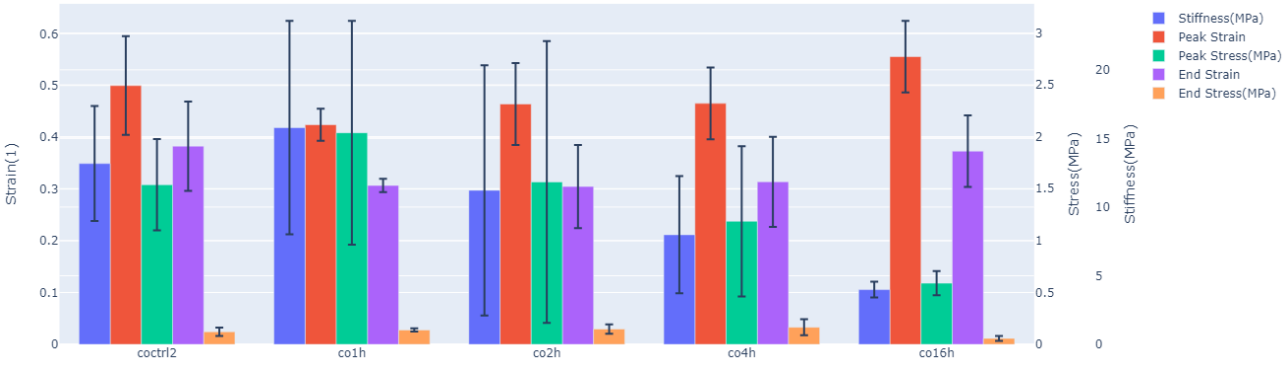

Figure 22: Average stiffness, strains and stresses for the collagen degraded groups

Firstly figure 22 shows the average stiffness for the groups of collagen degraded AC. The mean values with their standard deviations and p-values as compared to the control groups are shown in table 4. As can be seen from the figure and the table, the averages remain mainly constant throughout the groups. The only groups for which bigger changes in the stiffness can be observed are the 4 hour and 16 hour group. No significant changes were discovered for the stiffness of the collagen degraded AC, with the lowest p-value being 0.16667.

Secondly, figure 22 shows the average peak strain for the groups of collagen degraded AC. The mean values with their standard deviations and p-values as compared to the control groups are shown in table 4. A slight increase in the strain can be observed with increasing degradation time. Due to the large standard deviations the changes are however not significant with the smallest p-value being

Table 4: Data analysis results showing the mean + SD per group and their respective F and p-values with respect to the control group for the stiffness, peak strain, peak stress and end stress of the collagen degraded AC

Group	**Stiffness [MPa] (Mean + SD)**	**Stiffness (F-value; p-value)**	**Peak strain [1] (Mean + SD)**	**Peak strain (F-value; p-value)**	**Peak stress [MPa] (Mean + SD)**	**Peak stress (F-value; p-value)**	**End stress [MPa] (Mean + SD)**	**End Stress (F-value; p-value)**
Control	13.173 ± 4.191	n/a	0.450 ± 0.095	n/a	1.537 ± 0.440	n/a	0.121 ± 0.040	n/a
1 hour degraded	15.789 ± 7.779	6.0; 0.54762	0.424 ± 0.031	12.0; 0.54762	2.038 ± 1.078	6.0; 0.54762	0.139 ± 0.015	6.0; 0.54762
2 hour degraded	11.224 ± 9.116	10.0; 0.90476	0.464 ± 0.079	9.0; 1.00000	1.564 ± 1.357	10.0; 0.90476	0.147 ± 0.045	8.0; 0.90476
4 hour degraded	7.985 ± 4.272	11.0; 0.71429	0.466 ± 0.069	9.0; 1.00000	1.186 ± 0.724	10.0; 0.90476	0.165 ± 0.077	7.0; 0.71429
16 hour degraded	3.985 ± 0.575	15.0; 0.16667	0.0.556 ± 0.069	5.0; 0.38095	0.589 ± 0.117	15.0; 0.16667	0.057 ± 0.023	**17.0; 0.04762**

0.38095 for the 16 hour degraded group.

Thirdly, figure 22 shows the average peak stress for the groups of collagen degraded AC. The mean values with their standard deviations and p-values as compared to the control groups are shown in table 4. A decrease of the peak stress can be observed in the 16 hour degraded group. It should also be noted that the standard deviation for the 16 hour degraded group has also decreased as compared to the other groups. Again no significant changes are observed with the smallest p-value being 0.16667 for the 16 hour degraded group.

Lastly, figure 22 shows the average end stress for the groups of collagen degraded AC. The mean values with their standard deviations and p-values as compared to the control groups are shown in table 4. The data follows the trend shown in figure 22 and the table of decreasing stress over degradation time. The p-value for the 16 hour group for this test did show significance with a p-value of 0.04762. However, after the Holm-Benferronii correction was applied, the corrected p-value did not show significance anymore.

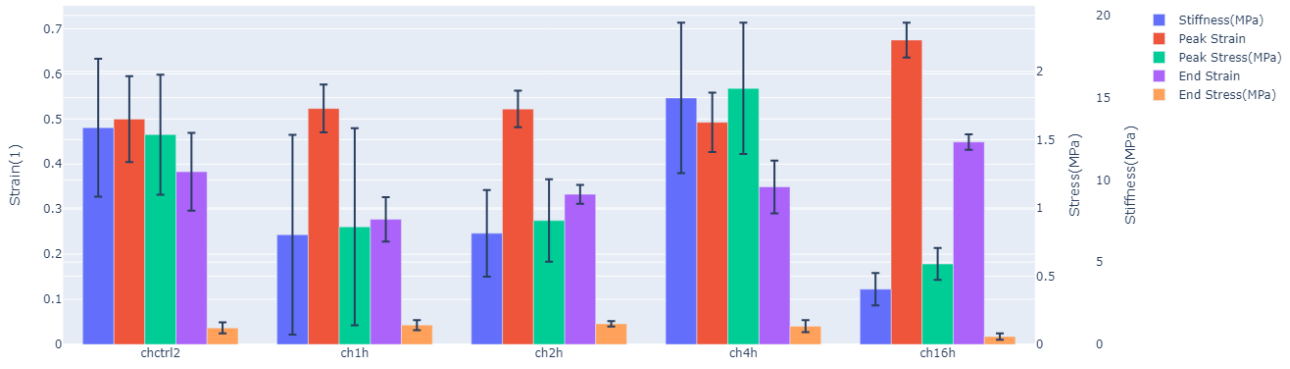

Figure 23: Average stiffness, strains and stresses for the GAG degraded groups

Firstly, figure 23 shows the average stiffness for the groups of GAG degraded AC. The mean values with their standard deviations and p-values as compared to the control groups are shown in table 5. The figure shows a large decrease in the stiffness of the material for the 16 hour degraded group going from a mean of 13.173 ± 4.191 to 3.358 ± 0.986. For the other groups the decrease is more subtle and the standard deviations are higher. Although the group shows a large difference, no significance was

Table 5: Data analysis results showing the mean + SD per group and their respective F and p-values with respect to the control group for the stiffness, peak strain, peak stress and end stress of the GAG degraded AC

Group	**Stiffness [MPa] (Mean + SD)**	**Stiffness (F-value; p-value)**	**Peak strain [1] (Mean + SD)**	**Peak strain (F-value; p-value)**	**Peak stress [MPa] (Mean + SD)**	**Peak stress (F-value; p-value)**	**End stress [MPa] (Mean + SD)**	**End Stress (F-value; p-value)**
Control	13.173 ± 4.191	n/a	0.450 ± 0.095	n/a	1.537 ± 0.440	n/a	0.121 ± 0.040	n/a
1 hour degraded	6.669 ± 6.070	17.0; 0.60000	0.523 ± 0.053	15.0; 0.86364	0.862 ± 0.721	16.0; 0.72727	0.142 ± 0.037	11.0; 0.72727
2 hour degraded	6.754 ± 2.631	16.0; 0.72727	0.522 ± 0.041	15.0; 0.86364	0.907 ± 0.302	16.0; 0.72727	0.151 ± 0.020	7.0; 0.28182
4 hour degraded	14.981 ± 4.574	5.0; 0.14545	0.493 ± 0.066	15.0; 0.86364	1.876 ± 0.481	3.0; 0.06364	0.134 ± 0.044	14.0; 1.00000
16 hour degraded	3.358 ± 0.986	21.0; 0.20909	0.675 ± 0.039	**0.0; 0.00909**	0.589 ± 0.117	20.0; 0.28182	0.057 ± 0.023	**26.0; 0.01818**

found after the Man-Whitney U test, showing a p-value of 0.20909.

Secondly, figure 23 shows the average peak strain for the groups of GAG degraded AC. The mean values with their standard deviations and p-values as compared to the control groups are shown in table 5. From the figure a slight increase in peak strain can be observed for the 16 hour degraded group. The mean changed from 0.450 ± 0.095 in the control group to 0.675 ± 0.039 in the 16 hour group, resulting in an average increase of 0.225 or 22.5%. The statistical test confirms this change to be significant with a value of $p = 0.00909$. After the Holm-Benferroni correction this significance was however rejected, as the target alpha became smaller than the given p-value.

Thirdly, figure 23 shows the average peak stress for the groups of GAG degraded AC. The mean values with their standard deviations and p-values as compared to the control groups are shown in table 5. The figure shows an increase in the peak stress for the 4 hour degraded group and a decrease for the other groups. The smallest p-value was found for the 4 hour degraded group, but this did not show significance even before the Holm-Benferroni correction. All other groups did not show significance as well.

Lastly, figure 23 shows the average end stress for the groups of GAG degraded AC. The mean values with their standard deviations and p-values as compared to the control groups are shown in table 5. The figure shows a clear decrease in the end stress for the 16 hour group. The mean value changed from 0.121 ± 0.040 MPa for the control group to 0.057 ± 0.023 MPa for the 16 hour group. This decrease was also shown to be significant by the Man-Whitney U test. With a p-value of 0.01818, the 16 hour group was shown to be significant before the Holm-Benferroni correction was conducted. After the correction, the significance was however rejected and no significant changes were found during the experiment.

5.2 Histology

The histology images along the longitudinal view are shown for both the collagen degraded AC and the GAG degraded AC. Considering the relaxation curves for the control, 1 hour and 2 hour groups were mostly similar, only the 4 hour, 16 hour and control group were stained. Figure 24 shows the collagen degraded AC and figure 25 shows the GAG degraded AC.

From the Alcian Blue staining in figure 24 a small decrease in GAG content can be observed in both the 4 hour and the 16 hour group by the lighter color of the staining near the surface of the AC.

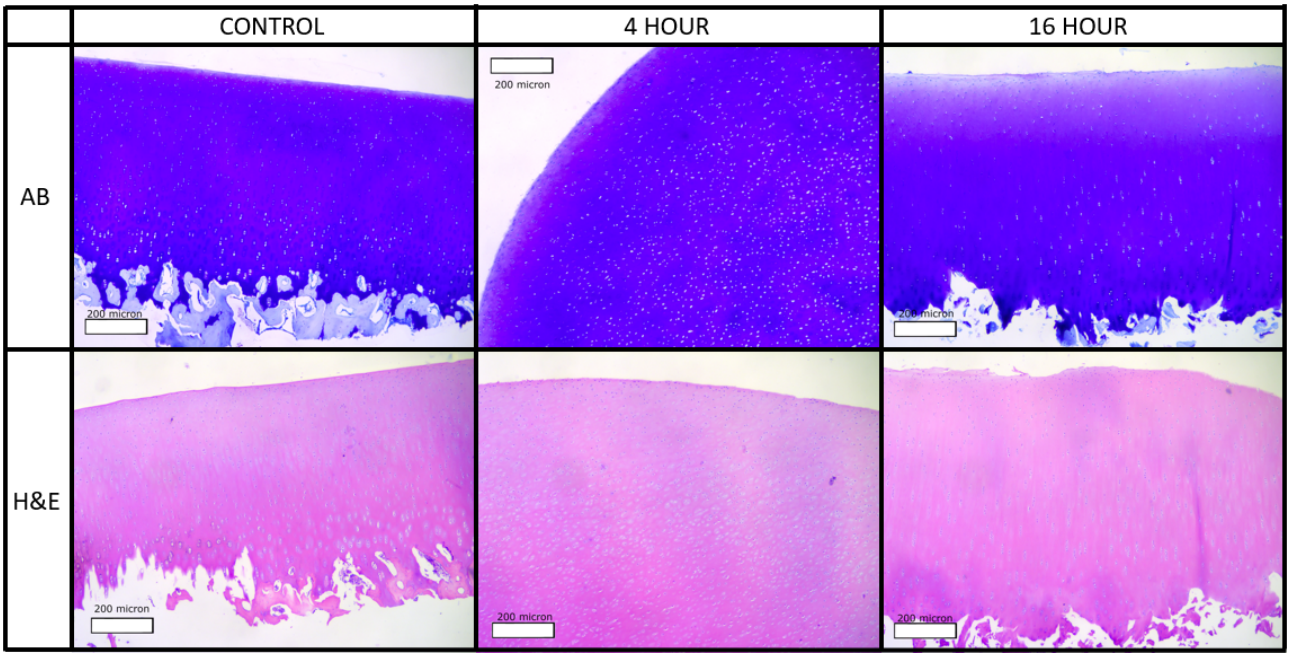

Figure 24: Staining results for collagen degraded AC. Leftmost column shows the type of staining, Alcian Blue or H&E; top row shows the degradation times; the scale shows the distance for 200 microns

Moreover, both groups show signs of collagen degradation on the surface, as the surface roughness increases as compared to the control group. This degradation is most notable in the 16 hour group, but at closer inspection the beginning of the degradation is visible for the 4 hour group. A decrease of ECM content can be observed along the surface of the AC with the H&E stained images. This is best observed in the 16 hour group, as the top layer of the AC is a slightly lighter shade and the dark brim along the surface of the AC has completely vanished. Finding the exact penetration depth of the enzyme is difficult using the supplied staining methods, as the entire ECM matrix is stained and isolating the collagen content proves to be difficult.

The Alcian Blue staining in figure 25 clearly shows the degradation of the GAGs in the AC. The 16 hour group shows a complete removal of the GAG content near the surface, with a gradient along the depth of the AC. This removal of the GAGs can be seen from the absence of blue in the image. From the image a penetration depth of 401 microns was found in the 16 hour group and 63 microns in the 4 hour group. This small penetration depth for the 4 hour group shows that the enzyme most likely takes around 4 hours to start degrading the material and no effect can be expected in the 1 hour and 2 hour groups. The H&E images also show the decrease in GAG content throughout the material as a lighter shade of coloring can be seen throughout the samples.

5.3 COMSOL

Some assumptions had to be made for the COMSOL models to relieve the optimization algorithm. The assumptions made are:

- Poisson ration ν is set to 0.45. Since cartilage is a biological material the value can range between 0.2-0.5[32].

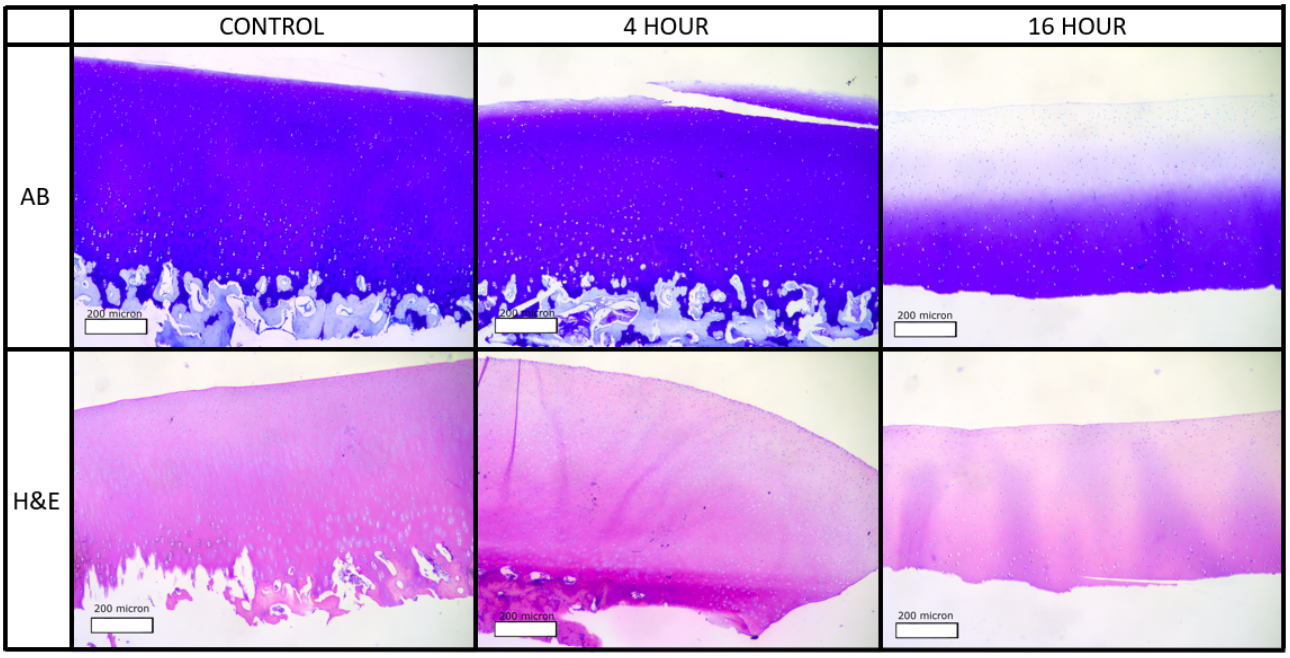

Figure 25: Staining results for collagen degraded AC. Leftmost column shows the type of staining, Alcian Blue or H&E; top row shows the degradation times; the scale shows the distance for 200 microns

- Density of the material is set to $1200 kg/m^3$[33].
- For synovial fluid the characteristics of water have been used.
- The permeability of the AC is set to $1E-15 m^4 N^{-1} s^{-1}$[34]
- Biot-Willis coefficient is set to 0.9.
- porosity is set to 0.9.

The thickness of the material matches the thickness of the plug to which the COMSOL model is fitted. In this case the thickness was 1.1 mm. An image of the model is shown in figure 26. The starting strain was obtained from the python software and also implemented into the model. Both the viscoelastic model and the poroviscoelastic model were optimized using the Matlab code and the curves shown in figure 27 were found. The poroviscoelastic model was fitted to solutions lasting 20 seconds to save time, but even with this the simulation took well over 20 minutes to run. The viscoelastic model was fitted following the simulation times as indicated by the methods section. Because the poroviscoelastic model was fitted over a shorter time period, the fit is less good. It can be seen however that even before the 20 seconds have been reached the model starts to deviate from the experimental data. The viscoelastic model could run a lot quicker with simulation times around 6 minutes and also shows a better fit. The RMSD obtained from this fit was $RMSD = 0.021779$, which shows a very small deviation from the experimental data. Considering the faster computation times and the higher precision of the viscoelastic model, the degraded AC has been fitted using the viscoelastic relaxation model. Table 6 shows the optimized Maxwell variables.

A second layer was introduced to the model to simulate the degraded AC. The degradation depths were obtained from figure 25 and converted to a percentile degradation using the thickness of the

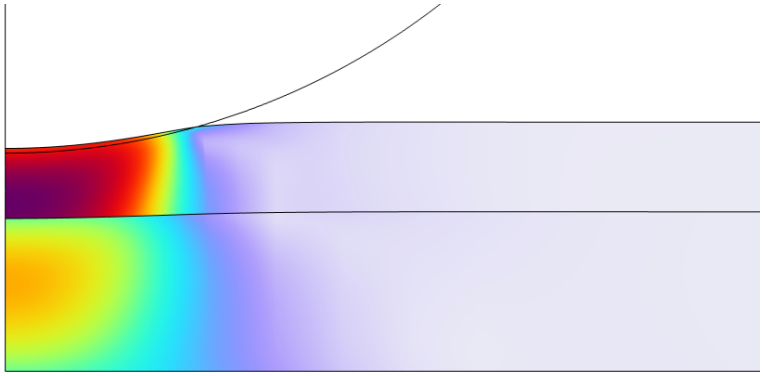

Figure 26: 2d-view of COMSOL model showing stresses caused by indentation

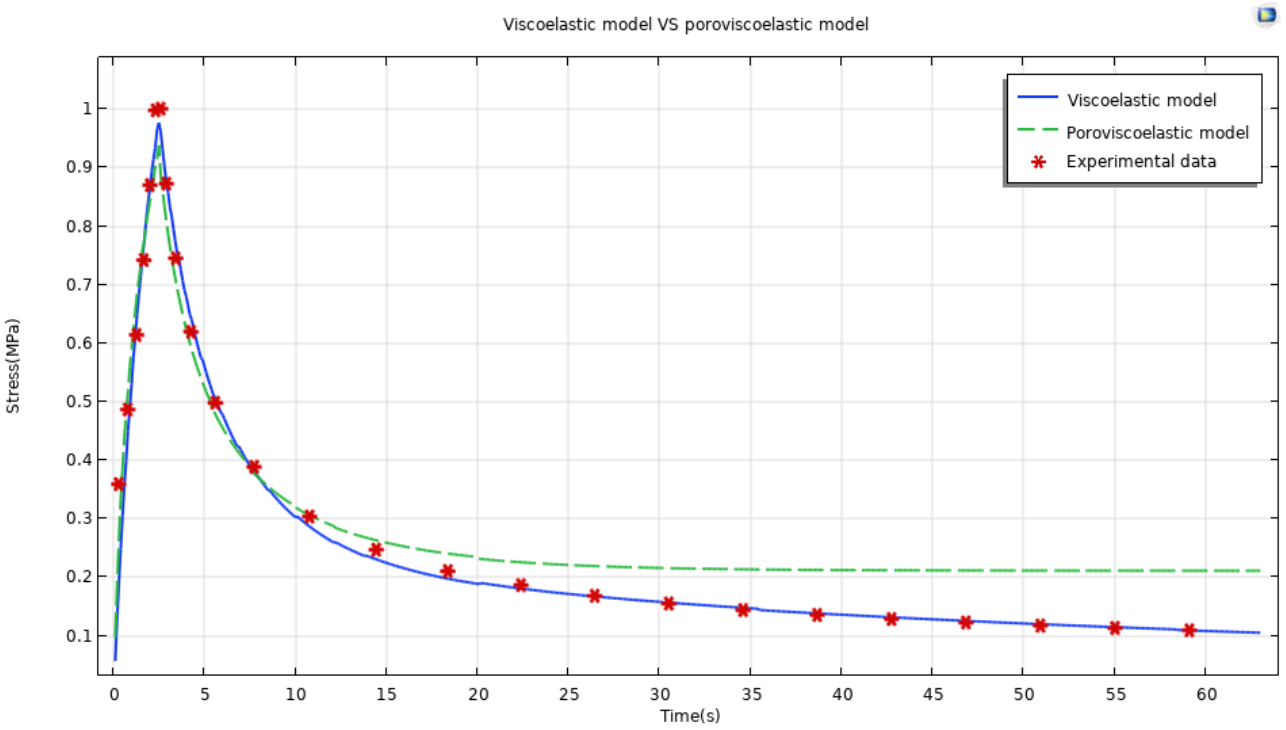

Figure 27: COMSOL fit to AC relaxation curve of healthy cartilage (t=1.1 mm)

stained samples. The bottom layer of the model used the variables shown in table 6. Since both samples were obtained from a plug with an AC thickness of 1.1 mm, the calculated degradation depths were:

- degradation depth 4h = $0.063/1.1 * 100 = 5.7\%$
- degradation depth 16h = $0.401/1.1 * 100 = 36.5\%$

The Maxwell variables were optimized using a 4 hour and 16 hour degraded experimental relaxation curve. The plugs had a thickness of $t = 1.1mm$, similar to the healthy cartilage. Both simulations were successfully optimized using their respective thicknesses ($t = 1.1mm$) and the Maxwell variables were obtained. The 4 hour degraded model showed an increase in the Young's Modulus and shear modulus of the viscoelastic model. The relaxation times did however decrease. The 16 hour degraded model showed similar relaxation times as the healthy cartilage. The Young's Modulus did however decrease

significantly. Both fits had a similar RMSD with $RMSD_{4h} = 0.033979$ and $RMSD_{16h} = 0.034056$. The obtained Maxwell variables are shown in table 6.

Table 6: Optimized Maxwell variables for the COMSOL models (t=1.1 mm)

Variable	**Healthy AC**	**4 hour GAG degraded AC**	**16 hour GAG degraded AC**
Young's Modulus (E)	0.4678[MPa]	0.5699 [MPa]	0.129958 [MPa]
Shear Modulus 1 (G1)	7.9989[MPa]	10.5884 [MPa]	9.997115 [MPa]
Relaxation time 1 (tau1)	3.1985[s]	1.3778 [s]	3.193710 [s]
Shear Modulus 2 (G2)	14.9996[MPa]	9.8985 [MPa]	9.99902 [MPa]
Relaxation time 2 (tau2)	0.9951[s]	0.9171 [s]	0.98550 [s]

6 Conclusion

After the experiments were conducted and the data was analyzed, significance was detected for peak strain and end stress of the 16 hour group of GAG degraded AC with p-values of 0.00909 and 0.01818 respectively. After the post-hoc correction this significance was however rejected and no significance was found between the groups.

Significance was also found for the 16 hour collagen degraded AC group. A p-value of 0.04762 was found for the end stress, indicating a significant change. After post-hoc correction this significance was however also rejected.

From the experiments with the current degradation times of 1 hour, 2 hour, 4 hour and 16 hour no significant changes were found in the stiffness, relaxation times and stresses and strains of the AC.

The penetration depth of the chondroitinase ABC has been found for a 4 hour and 16 hour degradation time. The degradation depth of the collagenase was not possible to find due to the staining methods used. Considering the limited number of datapoints for the degradation depth no trendline could be discovered between the degradation time and depth.

A COMSOL model was successfully fitted to the relaxation curve data for 4 hour and 16 hour degraded groups. Both showed a small RMSD of 0.033979 and 0.034056 respectively over a time range of t=0 s to t=45 s. The optimized variables showed the expected decrease in the strength of the material, as the Young's modulus decreased from 0.4678 MPa to 0.129958 MPa between the healthy and 16 hour GAG degraded AC.

Although there is no clear characterization of the enzymatic breakdown of the AC, the results have shown some of the effects on the biomechanical behavior. First of all a decrease in Young's Modulus was observed in both the COMSOL models and the data analysis. Secondly, it was observed that this decrease in stiffness led to a decrease in stress and an increase in strain of the material. The relaxation times were shown to remain similar throughout the degradation process.

7 Discussion

Several issues were discovered during the thesis, which have led to a decrease in available data. One issue that was discovered has to do with the degradation times of the enzymes. From the data it was discovered that it takes approximately 4 hours before the enzyme will start working. Considering the selected degradation times were 1 hour, 2 hours, 4 hours and 16 hours, half of the groups researched during the experiment did not have enough time to start degrading the material. In future research the degradation times should be done in different intervals starting from 4 hours to obtain a clearer understanding of the speed at which the enzymes penetrate the material.

Another issue was discovered with the staining. Although the H&E gives a clear view of the ECM content concentrations, and as such also the changes in collagen concentration, a more specific staining method is required to accurately determine the penetration depth of the collagenase degradation over time. For future research a staining using Picrosirius Red is preferred as this gives a clearer indication of the penetration depth.

Due to the small sample sizes of n=3, no real significance was found. Increasing the sample size should give a more meaningful statistical result as a normal distribution may be assumed over an increasing sample size.

Furthermore the biological variance of the bovine cartilage has led to problems during the creep test. The loading of the cartilage is done over a period of 45 seconds. For some plugs the increase in load from 0.1 to 0.4 N could be done within this set time, however there were also some plugs that did not reach this load within the given time. This resulted in some gaps in the data, which are visible in figure 18 by the sudden increase in strain. Increasing this time to a minute or more may help prevent this from occurring by giving the material a little more time to relax.

8 Ethics Paragraph

Research ethics plays an integral part in maintaining the integrity, responsibility and credibility of scientific research and should be thoroughly considered during the course of a research. It consists of the principles and guidelines that govern the conduct of researchers, making sure the studies are conducted ethically and with respect for the right of the participants. Every research will be subjected to some ethical challenges and pitfalls and this thesis is no exception. It is of great importance that the most crucial challenges and pitfalls should be discovered and discussed to ensure the obtained knowledge is reliable, valid and socially responsible.

Considering the use of animal material during this research, it is of importance to think about the consequences for the animals. Will they suffer during the course of the research? Can the number of required sacrifices be reduced? These are all questions that should be considered. As bovine material from the butcher is used for this research, it brings with it the ethical concern if killing an animal is the humane thing to do. If we were to consider the animals, which are locked up only to be slaughtered, unhappy, would killing the animal not be the humane thing to do[35]? On the other hand one might argue that killing is inhumane as this would prevent the animal from experiencing any pleasure it could still have[36]. Since the animal would have been slaughtered either way, one might say the use of animal materials for research is the morally acceptable choice. To add to this, as animal material can be used, there is no need for the use of human material, which comes with many moral dilemmas. Furthermore, the suffering of these few animals may lead to a better understanding of the degradation of AC, which might help many people suffering from osteoarthritis with providing a better understanding of their disease.

Considering the use of biological materials, research safety is another challenge which should be taken into account. It will be of great importance to follow the safety guidelines given by the workplaces and datasheets of any and all materials used to prevent harm from occurring to yourself or colleagues. As during the cutting process of the bovine material biological matter will become airborne, proper ventilation is required to prevent the contamination of surrounding material. For the morally acceptable choice extra precautions should be taken to prevent any form of contamination. Following lab safety guidelines such as wearing lab coats, knowing the dangers of chemicals you are handling and wearing safety goggles is of utmost importance to achieve this[37].

The final point to consider is the code of conduct on research. This code of conduct states that all research should be truthful, careful, trustworthy and replicable[38]. Moreover, the urge of changing a result to further the research should be resisted. This urge is often related to a conflict of interest. For example a scientist might research the effectiveness of a cure made by the company in which they are employed. Following the rules stated in the code of conduct, a morally acceptable research can be conducted.

All in all, considering there is no conflict of interest, the code of conduct is being followed, lab safety is taken into account and the bovine materials obtained come from animals which would be butchered either way, the few ethical concerns are outweighed by the benefits that this research may bring to the understanding of the breakdown of AC by osteoarthritis.

Bibliography

[1] H. Long, Q. Liu, H. Yin, K. Wang, N. Diao, Y. Zhang, J. Lin, and A. Guo, "Prevalence trends of site-specific osteoarthritis from 1990 to 2019: Findings from the global burden of disease study 2019," *Arthritis & Rheumatology*, vol. 74, no. 7, pp. 1172–1183, 2022, visited on 10-3-2023. [Online]. Available: https://onlinelibrary.wiley.com/doi/abs/10.1002/art.42089

[2] K. Halonen, M. Mononen, J. Jurvelin, J. Töyräs, J. Salo, and R. Korhonen, "Deformation of articular cartilage during static loading of a knee joint – experimental and finite element analysis," *Journal of Biomechanics*, vol. 47, no. 10, pp. 2467–2474, 2014, visited on 13-3-2023. [Online]. Available: https://www.sciencedirect.com/science/article/pii/S0021929014002346

[3] R. K. Korhonen, M. S. Laasanen, J. Töyräs, R. Lappalainen, H. J. Helminen, and J. S. Jurvelin, "Fibril reinforced poroelastic model predicts specifically mechanical behavior of normal, proteoglycan depleted and collagen degraded articular cartilage," *Journal of Biomechanics*, vol. 36, no. 9, pp. 1373–1379, 2003, visited on 16-4-2023. [Online]. Available: https://www.sciencedirect.com/science/article/pii/S0021929003000691

[4] A. Fox, A. Bedi, and S. Rodeo, "The basic science of articular cartilage: Structure, composition, and function," *Sports health*, vol. 1, pp. 461–8, 11 2009, visited on 13-03-2023.

[5] B. He, J. Wu, T. Kirk, J. Carrino, C. Xiang, and J. Xu, "High-resolution measurements of the multilayer ultra-structure of articular cartilage and their translational potential," *Arthritis research & therapy*, vol. 16, p. 205, 03 2014, visited on 13-03-2023.

[6] J. Eschweiler, N. Horn, B. Rath, M. Betsch, A. Baroncini, M. Tingart, and F. Migliorini, "The biomechanics of cartilage—an overview," *Life*, vol. 11, p. 302, 04 2021, visited on 08-07-2023.

[7] K. E. Chappell, A. A. Williams, and C. R. Chu, *Quantitative Magnetic Resonance Imaging of Articular Cartilage Structure and Biology*. Cham: Springer International Publishing, 2021, pp. 37–50, visited on 13-07-2023. [Online]. Available: https://doi.org/10.1007/978-3-030-78051-7_4

[8] P. Bruckner and M. van der Rest, "Structure and function of cartilage collagens," *Microscopy Research and Technique*, vol. 28, no. 5, pp. 378–384, 1994, visited on 13-03-2023. [Online]. Available: https://analyticalsciencejournals.onlinelibrary.wiley.com/doi/abs/10.1002/jemt.1070280504

[9] E. K. Moo, M. Ebrahimi, S. Sibole, P. Tanska, and R. Korhonen, "The intrinsic quality of proteoglycans, but not collagen fibres, degrades in osteoarthritic cartilage," *Acta Biomaterialia*, vol. 153, 09 2022, visited on 13-03-2023.

[10] N. P. Cohen, R. J. Foster, and V. C. Mow, "Composition and dynamics of articular cartilage: Structure, function, and maintaining healthy state," *Journal of Orthopaedic & Sports Physical Therapy*, vol. 28, no. 4, pp. 203–215, 1998, pMID: 9785256, Visited on 13-03-2023. [Online]. Available: https://doi.org/10.2519/jospt.1998.28.4.203

[11] V. Mow and X. E. Guo, "Mechano-electrochemical properties of articular cartilage: Their inhomogeneities and anisotropies," *Annual review of biomedical engineering*, vol. 4, pp. 175–209, 02 2002, visited on 13-03-2023.

[12] C. R. Harrell, B. S. Markovic, C. Fellabaum, A. Arsenijevic, and V. Volarevic, "Mesenchymal stem cell-based therapy of osteoarthritis: Current knowledge and future perspectives," *Biomedicine & Pharmacotherapy*, vol. 109, pp. 2318–2326, 2019, visited on 08-07-2023. [Online]. Available: https://www.sciencedirect.com/science/article/pii/S0753332218343075

[13] V. jagota, A. Sethi, and D.-K. Kumar, "Finite element method: An overview," *Walailak Journal of Science & Technology*, vol. 10, pp. 1–8, 01 2013, visited on 28-3-2023.

[14] M. Freutel, H. Schmidt, L. Dürselen, A. Ignatius, and F. Galbusera, "Finite element modeling of soft tissues: Material models, tissue interaction and challenges," *Clinical Biomechanics*, vol. 29, no. 4, pp. 363–372, 2014, visited on 13-03-2023. [Online]. Available: https://www.sciencedirect.com/science/article/pii/S0268003314000102

[15] H. Guo, S. A. Maher, and P. A. Torzilli, "A biphasic finite element study on the role of the articular cartilage superficial zone in confined compression," *Journal of Biomechanics*, vol. 48, no. 1, pp. 166–170, 2015, visited on 13-3-2023. [Online]. Available: https://www.sciencedirect.com/science/article/pii/S0021929014005958

[16] C. Schippers, L. Tsarkova, T. Bahners, J. Gutmann, and E. Cleve, "Improved maxwell model approach and its applicability toward lifetime prediction of biobased viscoelastic fibers," *Macromolecular Materials and Engineering*, vol. 306, p. 2100443, 09 2021, visited on 08-07-2023.

[17] Polymerdatabase.com, "Maxwell and voigt elements," 2022, visited on 08-07-2023. [Online]. Available: https://polymerdatabase.com/polymer%20physics/Maxwell-Kelvin.html

[18] BorgQueen, "Maxwell material," Dec 2022, visited on 08-07-2023. [Online]. Available: https://en.wikipedia.org/wiki/Maxwell_material

[19] Jan 2023, visited on 08-07-2023. [Online]. Available: $https://en.wikipedia.org/wiki/Kelvin%E2%80%93Voigt_material$

[20] Comsol, "Darcy's law — equation formulation," 2021, visited on 08-07-2023. [Online]. Available: $https://doc.comsol.com/5.6/doc/com.comsol.help.cfd/cfd_ug_fluidflow_porous.10.69.html$

[21] K. Vlees, "Kroon vlees vorstelijk vlees van eigen bodem," 2023, visited on 08-07-2023. [Online]. Available: https://www.kroonvlees.nl/over-kroon-vlees

[22] H. I. Limited, "Osteochondral allograft plugs," May 2023, visited on 14-07-2023. [Online]. Available: https://www.hospitalinnovations.com/products/osteochondral-plugs/

[23] Bruker, "Umt tribolab," 2023, visited on 14-07-2023. [Online]. Available: https://www.bruker.com/en/products-and-solutions/test-and-measurement/tribometers-and-mechanical-testers/umt-tribolab.html

[24] J. Bleyer, *Numerical Tours of Computational Mechanics with FEniCS*, https://comet-fenics.readthedocs.io, 2018, visited on 14-07-2023.

[25] H. Ghaednia, R. Jackson, H. Lee, A. Rostami, and X. Wang, *Contact Mechanics*, 11 2013, pp. 93–140, visited on 14-07-2023.

[26] A. Ganti, "Degrees of freedom in statistics explained: Formula and example," Apr 2023, visited on 14-07-2023. [Online]. Available: https://www.investopedia.com/terms/d/degrees-of-freedom.asp

[27] S. Alburger, "How to compute a population mean," Mar 2019, visited on 14-07-2023. [Online]. Available: https://sciencing.com/compute-population-mean-7199453.html

[28] I. Dinov, "F-distribution tables," May 2020, visited on 14-07-2023. [Online]. Available: $http://www.socr.ucla.edu/Applets.dir/F_Table.html$

[29] W. Haynes, *Holm's Method*. New York, NY: Springer New York, 2013, pp. 902–902, visited on 08-07-2023. [Online]. Available: $https://doi.org/10.1007/978-1-4419-9863-7_1214$

[30] Comsol, 2021, visited on 08-07-2023. [Online]. Available: https://doc.comsol.com/5.5/doc/com.comsol.help.sme/sme_ug_theory.06.26.html#3440773

[31] Matlab, "fmincon," 2023, visited on 08-07-2023. [Online]. Available: https://nl.mathworks.com/help/optim/ug/fmincon.html

[32] W. Zhang, P. Soman, K. Meggs, X. Qu, and S. Chen, "Tuning the poisson's ratio of biomaterials for investigating cellular response," *Advanced functional materials*, vol. 23, pp. 3226–3232, 07 2013, visited on 08-07-2023.

[33] C. Liu, M. Singh, J. Li, Z. Han, C. Wu, S. Wang, E. Sobol, V. Tuchin, M. Twa, and K. Larin, "Quantitative assessment of hyaline cartilage elasticity during optical clearing using optical coherence elastography," *Modern Technologies in Medicine*, vol. 7, pp. 44–51, 11 2014, visited on 08-07-2023.

[34] F. Boschetti, G. M. Peretti, M. Colombo, S. Cattaneo, R. Pietrabissa, F. Gervaso, and G. Fraschini, "Direct and indirect measurement of human articular cartilage permeability," 2004, visited on 14-07-2023.

[35] C. Belshaw, "32Death, Pain, and Animal Life," in *The Ethics of Killing Animals*. Oxford University Press, 11 2015, visited on 08-07-2023. [Online]. Available: https://doi.org/10.1093/acprof:oso/9780199396078.003.0003

[36] R. Lazo, "Value, time, and existence: Debates in the ethics of killing animals," *Journal of Animal Ethics*, vol. 7, no. 2, pp. 190–197, 2017, visited on 08-07-2023. [Online]. Available: https://www.jstor.org/stable/10.5406/janimalethics.7.2.0190

[37] M. Malik, "General and chemical laboratory safety," 09 2014, visited on 08-07-2023.

[38] V. van Universiteiten (VSNU), "De nederlands gedragscode wetenschapsbeoefening," 2014, visited on 08-07-2023.

Appendices

A Appendix A: Python code

The full python code can be found in the UMT-Data-analysis-V3.ipynb Google collaboratory notebook. The file can be found under the following link: https://colab.research.google.com/drive/1WlkXdNZpt2zye4GZFS4UTiRYdY-H_4q0?usp=sharing

B Appendix B: Matlab code

optimalization_algorithm.m

```
clc;
clear all;

import com.comsol.model.*
import com.comsol.model.util.*

save(”log.mat”);

filename = ’relaxation_2layer.mph’;

T = readtable(’relaxdeg4h.csv’);
time = table2array(T(:,”Time_s_”));
k = find(time==45);
ref = table2array(T(1:k, ”Stress_MPa_”));
fun = @(x)simulationdeg(ref, filename, x);

options = optimoptions(’ga’,’PopulationSize’,10, ’CrossoverFraction’, 0.6);
numParams = 5;
A = [];
b = [];
Aeq = [];
beq = [];
lb = [0.8 2.0 2.0 2.0 0.5];
ub = [2.0 5.0 3.0 5.0 1.5];
nonlin = [];
clc;
diary;
disp(”Starting GA optimization...”);
out = ga(fun, numParams, A,b, Aeq, beq, lb, ub, nonlin, options);
save(”out.mat”, ”out”);
clc;
options = optimoptions(’fmincon’,’Display’,’final’,’Algorithm’,’sqp’,
’FiniteDifferenceStepSize’, 0.1); x0 = [0.569919 10.588434 1.377846 9.898507 0.917122];
A = [];
b = [];
```

```
Aeq = [];
beq = [];
lb = [0.4 2.0 1.0 2.0 0.5];
ub = [1.0 15.0 5.0 15.0 2.5];
nonlin = [];
diary(”fmincon”);
disp(”Starting fmincon optimization...”);
out = fmincon(fun,x0,A,b, Aeq, beq, lb, ub, nonlin, options);
save(”out.mat”, ”out”);

load(”out.mat”)

k = find(time==63);
time = table2array(T(1:10:k, ”Time_s_”));
ref = table2array(T(1:10:k, ”Stress_MPa_”));

model = mphload(filename);

model.sol(’sol1’).feature(’t1’).set(’tlist’, ’range(0,0.1,63)’);

val1 = strcat(num2str(out(1)),’[MPa]’);
val2 = strcat(num2str(out(2)),’[MPa]’);
val3 = strcat(num2str(out(3)),’[s]’);
val4 = strcat(num2str(out(4)),’[MPa]’);
val5 = strcat(num2str(out(5)),’[s]’);

model.component(’comp1’).material(’pmat1’).propertyGroup(’Enu’).set(’E’,
val1);
model.param.set(’shear_mod1’, val2);
model.param.set(’tau1’, val3);
model.param.set(’shear_mod2’, val4);
model.param.set(’tau2’, val5);

model.sol(’sol1’).runAll;

model.result.table(’tbl2’).clearTableData;
model.result.numerical(’gev1’).set(’table’, ’tbl2’);
model.result.numerical(’gev1’).setResult;

updated = mphtable(model, ’tbl2’);

Q = ref;
figure;
plot(time, Q, ’.’, updated.data(:,1), updated.data(:,2), ’-’);
legend([”Experimental data”, ”Simulation data”]);
```

simulation.m

```
function RMSD = simulation(ref, filename, x)
import com.comsol.model.*
import com.comsol.model.util.*

count = 1;
E = [1];
eta1 = [1];
tau1 = [1];
eta2 = [1];
tau2 = [1];
RMSD_log = [1];

load log.mat;

fprintf('
index = find(E == x(1) & eta1 == x(2) & tau1 == x(3) & eta2 == x(4) &
tau2 == x(5));
if( isempty(index)) RMSD = RMSD_log(index);
count = count + 1;
save('log.mat', 'count', 'E', 'eta1', 'tau1', 'eta2', 'tau2',
'RMSD_log');
fprintf('RMSD = else model = mphload(filename);

model.sol('sol1').feature('t1').set('tlist', 'range(0,0.1,20)');

val1 = strcat(num2str(x(1)),'[MPa]');
val2 = strcat(num2str(x(2)),'[MPa]');
val3 = strcat(num2str(x(3)),'[s]');
val4 = strcat(num2str(x(4)),'[MPa]');
val5 = strcat(num2str(x(5)),'[s]');


model.component('comp1').material('pmat1').propertyGroup('Enu').set('E', val1);
model.param.set('shear_mod1', val2);
model.param.set('tau1', val3);
model.param.set('shear_mod2', val4);
model.param.set('tau2', val5);

try
model.sol('sol1').runAll;

model.result.table('tbl2').clearTableData;
model.result.numerical('gev1').set('table', 'tbl2');
model.result.numerical('gev1').setResult;
```

```
updated = mphtable(model, 'tbl2');

k = find(updated.data(:,1)==0.1);
Q = ref(k:end);
Qest = updated.data(k:end,2);
T = length(Qest);
RMSD = sqrt(sum((Qest - Q).^2)/T);
fprintf('RMSD =
count = count + 1;
E = [E x(1)];
eta1 = [eta1 x(2)];
tau1 = [tau1 x(3)];
eta2 = [eta2 x(4)];
tau2 = [tau2 x(5)];
RMSD_log = [RMSD_log RMSD];
save('log.mat', 'count', 'E', 'eta1', 'tau1', 'eta2', 'tau2',
'RMSD_log');
catch
fprintf('Failed to converge...');
count = count + 1;
RMSD = 100;
eta1 = [eta1 x(2)];
tau1 = [tau1 x(3)];
eta2 = [eta2 x(4)];
tau2 = [tau2 x(5)];
RMSD_log = [RMSD_log RMSD];
save('log.mat', 'count', 'E', 'eta1', 'tau1', 'eta2', 'tau2', 'RMSD_log');
end
end
end
```

simulationDeg.m

```
function RMSD = simulationdeg(ref, filename, x)
import com.comsol.model.*
import com.comsol.model.util.*

count = 1;
E = [1];
eta1 = [1];
tau1 = [1];
eta2 = [1];
tau2 = [1];
RMSD_log = [1];

load log.mat;

fprintf('
index = find(E == x(1) & eta1 == x(2) & tau1 == x(3) & eta2 == x(4) & tau2 == x(5));
if( isempty(index)) RMSD = RMSD_log(index);
count = count + 1;
save('log.mat', 'count', 'E', 'eta1', 'tau1', 'eta2', 'tau2', 'RMSD_log');
fprintf('RMSD = else model = mphload(filename);

model.sol('sol1').feature('t1').set('tlist', 'range(0,0.1,45)');

val1 = strcat(num2str(x(1)),'[MPa]');
val2 = strcat(num2str(x(2)),'[MPa]');
val3 = strcat(num2str(x(3)),'[s]');
val4 = strcat(num2str(x(4)),'[MPa]');
val5 = strcat(num2str(x(5)),'[s]');

model.param.set('deg_depth', 'thickness*0.057');
model.component('comp1').material('pmat1').propertyGroup('Enu').set('E', val1);
model.param.set('shear_modDeg1', val2);
model.param.set('tauDeg1', val3);
model.param.set('shear_modDeg2', val4);
model.param.set('tauDeg2', val5);

try
model.sol('sol1').runAll;

model.result.table('tbl2').clearTableData;
model.result.numerical('gev1').set('table', 'tbl2');
model.result.numerical('gev1').setResult;

updated = mphtable(model, 'tbl2');
```

```
k = find(updated.data(:,1)==0.1);
Q = ref(k:end);
Qest = updated.data(k:end,2);
T = length(Qest);
RMSD = sqrt(sum((Qest - Q).^2)/T);
fprintf('RMSD =
count = count + 1;
E = [E x(1)];
eta1 = [eta1 x(2)];
tau1 = [tau1 x(3)];
eta2 = [eta2 x(4)];
tau2 = [tau2 x(5)];
RMSD_log = [RMSD_log RMSD];
save('log.mat', 'count', 'E', 'eta1', 'tau1', 'eta2', 'tau2', 'RMSD_log');
catch
fprintf('Failed to converge...');
count = count + 1;
RMSD = 100;
eta1 = [eta1 x(2)];
tau1 = [tau1 x(3)];
eta2 = [eta2 x(4)];
tau2 = [tau2 x(5)];
RMSD_log = [RMSD_log RMSD];
save('log.mat', 'count', 'E', 'eta1', 'tau1', 'eta2', 'tau2', 'RMSD_log');
end
end
end
```

C Appendix C: Experimental data

	Name	Stiffness(MPa)	Label	Tau Creep(s)	Peak Strain	End Strain	Strain Reduction(%)	Tau Relax(s)	Peak Stress(MPa)	End Stress(MPa)	Stress Reduction(%)
0	co16h-1	4.739583838	co16h	505.5214726	0.6216835531	0.4637668864	25.40145479	17.09343816	0.7355529897	0.02627776643	96.42748153
1	co16h-2	3.346921321	co16h	2000	0.5854724356	0.3597032048	38.56188901	22.26786131	0.5811026904	0.08200960641	85.88724372
2	co16h-3	3.868012373	co16h	237.556147	0.4603585277	0.2962408806	35.64996349	28.12401681	0.4498462413	0.0643982874	85.68755965
3	co1h-1	7.373122446	co1h	333.2081796	0.4665908813	0.3140908813	32.6838792	21.40341126	0.9483989177	0.1595164159	83.1804515
4	co1h-2	13.8620629	co1h	468.4074693	0.413694458	0.317756958	23.19042427	16.97362369	1.659683921	0.1246112393	92.49186922
5	co1h-3	26.13188557	co1h	207.2720202	0.3926687387	0.2888225849	26.44624937	14.27439566	3.506196381	0.1319028155	96.23800834
6	co2h-1	4.239272189	co2h	298.7584715	0.5717330933	0.4060188075	28.98455375	18.50673852	0.5976847374	0.0855097282	85.69317185
7	co2h-2	5.332712877	co2h	1014.300486	0.3828907686	0.2090672392	45.39768092	13.40671029	0.6122309136	0.1635238471	73.2904949
8	co2h-3	24.10042474	co2h	203.4181554	0.4382058438	0.2995694802	31.6372694	5	3.482768974	0.1928493862	94.46275686
9	co4h-1	4.001235959	co4h	847.3845984	0.4345316739	0.2734205627	37.07695452	27.18357785	0.5310974 67	0.1278867741	75.92028168
10	co4h-2	6.043946648	co4h	259.6772282	0.5617493508	0.434931169	22.57558138	21.53128331	0.8309185491	0.0942069445 8	88.66231297
11	co4h-3	13.90972855	co4h	235.2884084	0.4002252197	0.2335585531	41.64321948	26.75723525	2.194678526	0.272042973 2	87.60442726
12	coctrl1-1	8.100800379	coctrl1	215.885402	0.5571313477	0.4362222567	21.70208002	20.51906252	1.067364861	0.105669069	90.10000489
13	coctrl1-2	1.468421932	coctrl1	2000	0.4987919399	0.2649824161	46.87516079	29.95467908	0.2140356266	0.0878033093 8	58.97724561
14	coctrl1-3	10.42109294	coctrl1	402.1049962	0.3434501648	0.1781376648	48.1328929	23.70313 25	1.319333573	0.3055688001	76.83915529
15	coctrl2-4	12.0499262	coctrl2	1999.999958	0.6062130127	0.4757130127	21.52708656	16.09893409	1.677418427	0.114112690 6	93.1971243
16	coctrl2-5	8.694956536	coctrl2	263.8553127	0.5184270301	0.405350107	21.81154078	17.50914116	0.9419235534	0.075183630 99	92.01807506
17	coctrl2-6	18.77374806	coctrl2	239.4870899	0.3749779402	0.267835083	28.57310942	19.99236471	1.990936258	0.173174694 3	91.30184638

Figure 28: Collagen degraded AC analysis data

	Name	Stiffness(MPa)	Label	Tau Creep(s)	Peak Strain	End Strain	Strain Reduction(%)	Tau Relax(s)	Peak Stress(MPa)	End Stress(MPa)	Stress Reduction(%)
0	ch16h-1	4.739583838	ch16h	505.5214726	0.6216835531	0.4637668864	25.40145479	17.09343816	0.7355529897	0.02627776643	96.42748153
1	ch16h-2	2.832010382	ch16h	1999.999998	0.6919216919	0.4251035101	38.56190447	22.26786133	0.5811034766	0.08200971651	85.88724387
2	ch16h-3	2.502831521	ch16h	704.5685565	0.7114632901	0.4578269265	35.64995793	28.12401641	0.4499459648	0.06439824818	85.68755957
3	ch1h-1	1.427359874	ch1h	263.1232577	0.5981262533	0.2904595866	51.43841538	24.03698306	0.2303792613	0.09010470422	60.88853497
4	ch1h-2	15.17719751	ch1h	206.9711862	0.4838645534	0.3299515099	31.80911733	16.68340173	1.87129176	0.1624986685	91.31623021
5	ch1h-3	3.402542537	ch1h	266.8255363	0.4878260498	0.2118260498	56.57754442	36.74218224	0.4829916993	0.1729226587	64.19759202
6	ch2h-1	3.834889536	ch2h	285.7585673	0.5749234244	0.354538809	38.33286418	22.29401902	0.5518151111	0.1289650056	76.62894637
7	ch2h-2	6.215699461	ch2h	230.7278709	0.5150596619	0.3046429952	40.85287244	20.81581697	0.879721535	0.1771792805	79.85961768
8	ch2h-3	10.21073191	ch2h	228.2835069	0.4762953127	0.3393722358	28.74751719	20.46948086	1.290238948	0.1480844789	88.52270898
9	ch4h-1	8.554756508	ch4h	202.9974155	0.5858602246	0.4320802246	26.2133169	20.79131235	1.201594957	0.1114428863	90.75038675
10	ch4h-2	17.55875203	ch4h	377.7538471	0.4382030741	0.3107030741	29.09609894	17.87018606	2.132671993	0.09490621392	95.54989167
11	ch4h-3	18.82969189	ch4h	232.1595914	0.4541133626	0.3053633626	32.75613806	16.12176023	2.292579678	0.1954593206	91.47426271
12	chctrl1-1	5.160650031	chctrl1	252.3828363	0.4957058716	0.3024915859	38.97760684	50	0.7016668122	0.1606396945	77.10598652
13	chctrl1-2	8.441552204	chctrl1	227.6017618	0.5813499451	0.4349863087	25.1765116	18.12972531	1.140134328	0.1249723525	89.03880452
14	chctrl1-3	2.288386029	chctrl1	272.9468582	0.583470296	0.329580363	43.49214892	26.87625409	0.3385435239	0.1199887089	64.55737581
15	chctrl2-4	12.0499262	chctrl2	1999.999958	0.6062130127	0.4757130127	21.52708656	16.09893409	1.677418427	0.1141126906	93.1971243
16	chctrl2-5	8.694956536	chctrl2	283.8553127	0.5184270301	0.405350107	21.81154078	17.50914116	0.9419235534	0.07518363099	92.01807506
17	chctrl2-6	18.77374806	chctrl2	239.4870899	0.3749779402	0.267835083	28.57310942	19.99236471	1.990936258	0.1731746943	91.30184638
18	chctrl3-7	8.100800379	chctrl3	215.885402	0.5571313477	0.4362222567	21.70208002	20.51906252	1.067364861	0.105669069	90.10000489
19	chctrl3-8	1.468421932	chctrl3	2000	0.4987919399	0.2649824161	46.87516079	29.95467908	0.2140356266	0.08780330938	58.97724561
20	chctrl3-9	10.42109294	chctrl3	402.1049962	0.3434501648	0.1781376648	48.1328929	23.7031325	1.319333573	0.3055688001	76.83915529

Figure 29: GAG degraded AC analysis data